JCB Journal of Cell Biology

ARTICLE

# Competition between two phosphatases fine-tunes Hedgehog signaling

Min Liu[1,2*], Aiguo Liu[1,2*], Jie Wang[1*], Yansong Zhang[1], Yajuan Li[1], Ying Su[3], and Alan Jian Zhu[1,2]

**Hedgehog (Hh) signaling is essential for embryonic development and adult homeostasis. How its signaling activity is fine-tuned in response to fluctuated Hh gradient is less known. Here, we identify protein phosphatase V (PpV), the catalytic subunit of protein phosphatase 6, as a homeostatic regulator of Hh signaling. *PpV* is genetically upstream of *widerborst* (*wdb*), which encodes a regulatory subunit of PP2A that modulates high-level Hh signaling. We show that PpV negatively regulates Wdb stability independent of phosphatase activity of PpV, by competing with the catalytic subunit of PP2A for Wdb association, leading to Wdb ubiquitination and subsequent proteasomal degradation. Thus, regulated Wdb stability, maintained through competition between two closely related phosphatases, ensures graded Hh signaling. Interestingly, *PpV* expression is regulated by Hh signaling. Therefore, *PpV* functions as a Hh activity sensor that regulates Wdb-mediated PP2A activity through feedback mechanisms to maintain Hh signaling homeostasis.**

## Introduction

Hedgehog (Hh) signaling is an evolutionarily highly conserved signaling cascade that coordinates cell fate decisions, tissue patterning, organ growth, and adult homeostasis (Lee et al., 2016). Dysregulated Hh signaling in humans leads to birth defects and cancer (Pak and Segal, 2016; Kong et al., 2019). Thus, the level as well as the activity of core signaling components must be precisely regulated in order to maintain homeostasis of Hh signaling (Pak and Segal, 2016; Liu, 2019). Among identified homeostatic regulatory machineries, posttranslational modifications (PTM) play critical roles in modulating the configuration, subcellular localization, physical interaction, and molecular functions of the core players (Barber and Rinehart, 2018). Thus, various forms of PTM significantly expand cellular properties of key signaling players of the Hh regulatory network in development and adult homeostasis.

Phosphorylation, a common PTM event occurring in >30% of human proteins (Cohen, 2002; Vlastaridis et al., 2017), is tightly regulated by opposing activities of specific protein kinases and phosphatases. They often act together in development to provide dynamic yet robust regulation on the abundance and activity of core players of developmental signaling, forming feedback or feed-forward regulatory networks to maintain signaling homeostasis (Couzens et al., 2013; Xu et al., 2016; Thompson and Williams, 2018). Extensive studies uncovered a stereotypical sequential phosphorylation profile of Hh signaling activator Smoothened (Smo), comprised of basal-, moderate- and highly phosphorylated Smo species, and showed that it is essential for Hh signal transduction in *Drosophila melanogaster* (Jia et al., 2004; Zhang et al., 2004; Apionishev et al., 2005; Su et al., 2011; Li et al., 2016). Sequential Smo phosphorylation is catalyzed first by cyclic adenosine 3′, 5′-monophosphate–dependent protein kinase A, followed by casein kinase I. In addition, phosphorylation by G protein–coupled receptor kinase 2 is required for maximal Smo activity and subsequent Smo internalization and degradation (Chen et al., 2010; Maier et al., 2014). Two protein serine/threonine phosphatases, namely protein phosphatase 1 and 2A (PP2A), act as Smo-specific phosphatases that respectively antagonize cyclic adenosine 3′, 5′-monophosphate–dependent protein kinase A and casein kinase I activities to maintain sequential phosphorylation of Smo (Su et al., 2011). However, how such Smo-associated kinases and phosphatases sense Hh signaling gradient and how they in turn collectively coordinate graded Smo phosphorylation are not well understood.

Here, we provide genetic and biochemical evidence demonstrating that protein phosphatase V (PpV), the *Drosophila* orthologue of the catalytic subunit of protein phosphatase 6 (PP6C), is a bona fide Hh signaling target whose activity is

[1]Ministry of Education Key Laboratory of Cell Proliferation and Differentiation, School of Life Sciences, Peking University, Beijing, China; [2]Peking-Tsinghua Center for Life Sciences, Academy for Advanced Interdisciplinary Studies, Peking University, Beijing, China; [3]Institute of Evolution and Marine Biodiversity, Ocean University of China, Qingdao, China.

*M. Liu, A. Liu, and J. Wang contributed equally to this paper; Correspondence to Ying Su: suying@ouc.edu.cn; Alan Jian Zhu: zhua@pku.edu.cn.

essential for regulating PP2A stability in response to differential Hh signaling. Importantly, our study uncovers a noncanonical regulatory function of PpV that does not require its phosphatase activity. Instead, it competes with the catalytic subunit of PP2A for association with Widerborst (Wdb), one of four variable regulatory subunits of PP2A heterotrimeric holoenzyme. The resulting noncanonical Wdb/PpV complex is not functional, leading to Wdb degradation in the proteasome. Our results suggest that *PpV* senses graded Hh signaling activity to maintain a stereotypical Smo phosphorylation profile essential for Hh signaling. As the expression of *PpV* directly responds to differential Hh signaling gradient, our study highlights the importance of feedback regulation of *PpV* on Wdb-mediated PP2A phosphatase activity in homeostatic regulation of Hh signaling.

## Results

### Identification of the PpV phosphatase as a positive regulator of Hh signaling

Hh signaling is one of the major signaling systems that pattern the *Drosophila* wing, playing a key role in determining the distance between L3 and L4 (L3-L4) longitudinal veins (Fig. 1 A). In an in vivo RNAi screen, we found that knocking down the *PpV* phosphatase resulted in reduced L3-L4 distance in the adult wing blade (Fig. 1, C and F), a phenotype which has been previously observed in several conditions of reduced Hh signaling, for example, by overexpressing *patched* (*ptc*), a negative regulator of Hh signaling (Fig. 1 B and Fig. S1 C). Reduced *PpV* expression also resulted in loss of anterior cross-vein, a phenotype consistent with a reported role of *PpV* in JNK-dependent tumor progression (Ma et al., 2017). However, loss of anterior cross-vein, but not reduced L3-L4 distance, was partially suppressed in *PpV* RNAi adult wings by increased activity of *puckered* (*puc*; Fig. 1, D and E), a negative regulator of JNK signaling, suggesting that *PpV* plays an additional role in Hh signaling. This notion was further supported by observed genetic interactions between *PpV* and core components of Hh signaling: the wing defects induced by reduced expression of *cubitus interruptus* (*ci*; Fig. S1 A), the Hh signaling transcription factor, or by overexpressing *ptc* (Fig. S1 C), were further enhanced by *PpV* RNAi (Fig. S1, B and D). Consistently, the fusion of proximal L3 and L4 veins in a temperature-sensitive *ci* mutant ($ci^{cell}$) background (Fig. S1, E–G′; Slusarski et al., 1995; Méthot and Basler, 1999) became more prominent when one copy of *PpV* was removed in a heterozygous $PpV^{KO}$ background (Fig. S1, H and H′; cf. Fig. S1, F and F′). Together, the above results establish a requirement of *PpV* activity in mediating Hh signaling in *Drosophila* wing development.

To confirm that Hh signaling was indeed altered when *PpV* was dysfunctional, we examined third instar larval wing imaginal discs for stability of full-length Ci (CiFL), as well as expression of Hh signaling responsive genes *decapentaplegic* (*dpp*) and *collier/knot* (*col*), which differentially respond to graded Hh morphogen concentration. Low-level Hh signaling was sufficient to stabilize CiFL (Fig. 1 G), whereas *dpp* (Fig. 1 H) and *col* (Fig. 1 I) were induced by intermediate and high levels of Hh activity, respectively, consistent with a previous report (Torroja et al., 2005). Considering that the L3-L4 intervein region is largely maintained by *col* activation (Crozatier et al., 2002, 2003), it is not surprising that the production of Col protein was diminished when *PpV* activity was reduced (Fig. 1 L), demonstrating that *PpV* is required for high-level Hh activity. However, contrary to expectations, we found that CiFL protein was stabilized (Fig. 1 J) and the expression of *dpp*-lacZ was expanded to more anterior cells when *PpV* RNAi was expressed (Fig. 1 K). These surprising results suggest that *PpV* is also able to repress the expression of target genes responsive to low to intermediate levels of Hh signaling. To verify these apparently contradictory results, we generated a *PpV* null allele ($PpV^{KO}$) in which the coding sequence of *PpV* was removed by homologous recombination. Few hemizygous $PpV^{KO}$ males (<5%) survived to early pupal stage, thereby allowing us to examine the effect of *PpV* null on Hh signaling targets in larval wing discs. The result observed in $PpV^{KO}$ hemizygous wing discs was similar to that obtained with *PpV* RNAi (Fig. 1, M–R), highlighting a surprising role of *PpV* in differential regulation of Hh responsive genes.

### *PpV* acts upstream of *wdb* to control high-level Hh signaling

The defect induced by reduced *PpV* activity in adult wing highly resembled the phenotype caused by *wdb* overexpression. Wdb was identified in our previous study as a specific regulatory subunit that controls the activity of PP2A in Smo phosphorylation and Hh signaling activity (Su et al., 2011). Following either *wdb* overexpression or reduced *PpV* activity, the expression of low to intermediate levels of Hh targets was expanded, while the activation of high-level Hh targets was repressed. The similarity in phenotypes following the two manipulations led us to believe that these genes may function in the same pathway. To explore this possibility, we examined the epistatic relationship between *PpV* and *wdb*. We found that loss of both *wdb* and *PpV* expression in adult wing phenocopied the defect associated with *wdb* RNAi alone (Fig. 2, A–D), suggesting that *wdb* is epistatic to *PpV*. Consistently, loss of Col expression induced by *PpV* RNAi (Fig. 2 F′) in wing disc was rescued upon coexpression of a dominant negative form of *wdb* (*wdbDN*; Fig. 2 H′).

Previous studies provided extensive evidence for sequential phosphorylation and subsequent cell surface localization of Smo in mediating Hh signaling in *Drosophila* (Zhu et al., 2003; Jia et al., 2004; Zhang et al., 2004; Apionishev et al., 2005). Consistent with the report that Wdb-mediated PP2A phosphatase activity (Wdb-PP2A) directly dephosphorylates highly phosphorylated Smo to prevent over-activation of Hh signaling, knocking down *wdb* (Fig. 2, K–K′′ and M) behaved similarly to adding Hh (Fig. 2, I–J′′ and M) to *Drosophila* Schneider 2 (S2) cells to induce hyper-phosphorylation and translocation of Smo from cytosol to the plasma membrane. Similar effects on Smo were observed when *PpV* was overexpressed in S2 cells (Fig. 2, L–L′′ and M). Together, the above results demonstrate that *PpV* acts upstream of *wdb* to modulate Smo phosphorylation in Hh signaling.

### PpV regulates Wdb protein abundance

To determine how *PpV* regulates *wdb* activity, we first examined *wdb* expression in wing disc following alteration of *PpV* activity.

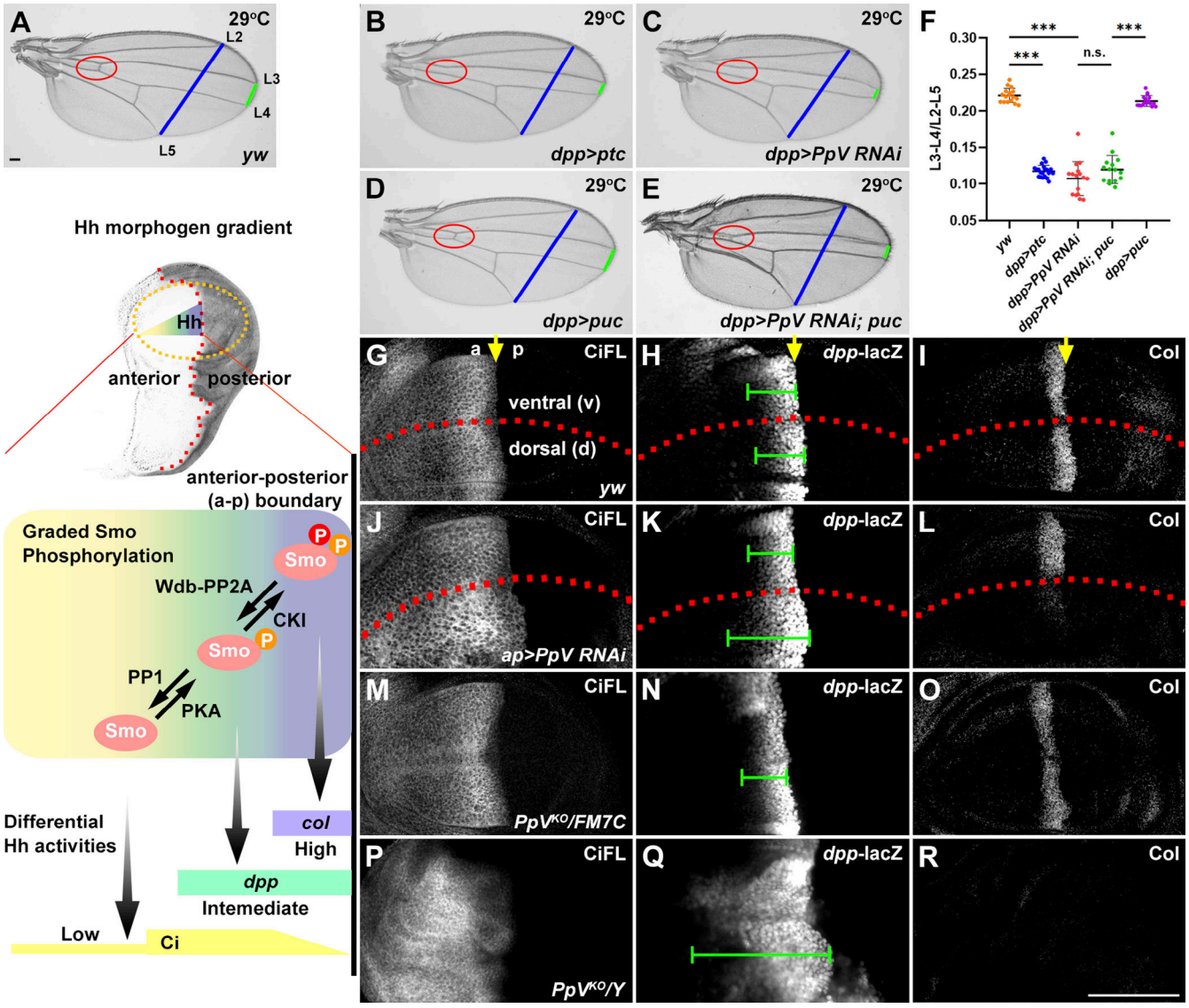


Figure 1. **PpV positively regulates Hh signaling. (A)** Shown are a WT adult wing blade and a third instar larval wing imaginal disc. Hh protein produced in posterior compartment of the wing disc diffuses into anterior compartment to pattern the wing pouch (circled by yellow dotted line), which eventually undergoes metamorphosis to form an adult wing blade. Sequential Smo phosphorylation by cyclic adenosine 3′, 5′-monophosphate–dependent protein kinase A (PKA) and casein kinase I (CKI) is required for Hh signaling, while protein phosphatase 1 (PP1) and PP2A, respectively, antagonize the PKA and CKI activities to transduce graded Hh signaling. Low-level Hh signaling is sufficient to stabilize CiFL, whereas *dpp* and *col* are induced by intermediate and high levels of Hh activity, respectively. **(B–E)** Overexpressing *ptc* (B) or *PpV* RNAi (C) by the *dpp*-Gal4 driver in the wing blade led to complete loss of anterior cross vein (ACV) and reduced L3-L4 distance. Ectopic *puc* expression driven by *dpp*-Gal4 (D) partially suppressed the loss of ACV phenotype but not the reduced L3-L4 distance caused by *PpV* RNAi (E). Red circles mark the position of the ACV. Green lines indicate the distance between distal ends of L3 and L4, while blue lines indicate the distance between L2 and L5. **(F)** Statistical analysis of the ratio of the distance between distal ends of L3 and L4 to the distance between distal ends of L2 and L5 shown in A–E. Data are presented as mean ± SD ($n^{yw}$ = 17, $n^{dpp>ptc}$ = 20, $n^{dpp>PpV\ RNAi}$ = 16, $n^{dpp>PpV\ RNAi;\ puc}$ = 15, $n^{dpp>puc}$ = 17). Two-tailed Student's *t* tests were used to analyze the difference between two different genotypes. ***, significant difference with a P value <0.001. n.s., no significant difference. **(G–R)** CiFL protein stabilization, *dpp*, and *col* transcription correlated with low, intermediate, and high levels of Hh signaling, respectively, abutting the a-p boundary (marked by yellow arrows) in WT (G–I) as well as in heterozygous *PpV* knockout ($PpV^{KO}$) wing discs (M–O). Reduced *PpV* expression in dorsal compartment by RNAi (J–L) or in hemizygous $PpV^{KO}$ wing discs (P–R) stabilized CiFL (J and P) and induced *dpp*-lacZ expression (K and Q) to a more anterior region. Note that *dpp*-lacZ (marked by green lines) was normally expressed in ∼10 rows of cells in WT (H), ventral (v) compartment (K), and heterozygous $PpV^{KO}$ wing discs (N). Its expression expanded to up to 20 rows in dorsal (d) compartment of wing discs expressing *PpV* RNAi by *ap*-Gal4 (K), or to the anterior-most region in $PpV^{KO}$ wing discs, where *PpV* expression was eliminated (Q). Contrary to the effect on CiFL and *dpp*-lacZ, Col expression along the a-p boundary was abolished by *PpV* RNAi (L) or in hemizygous $PpV^{KO}$ wing discs (R). The dorsal-ventral boundary is marked by a dotted red line. In this and all subsequent figures, wing discs are shown with anterior to the left and dorsal down. Scale bars, 100 µm.

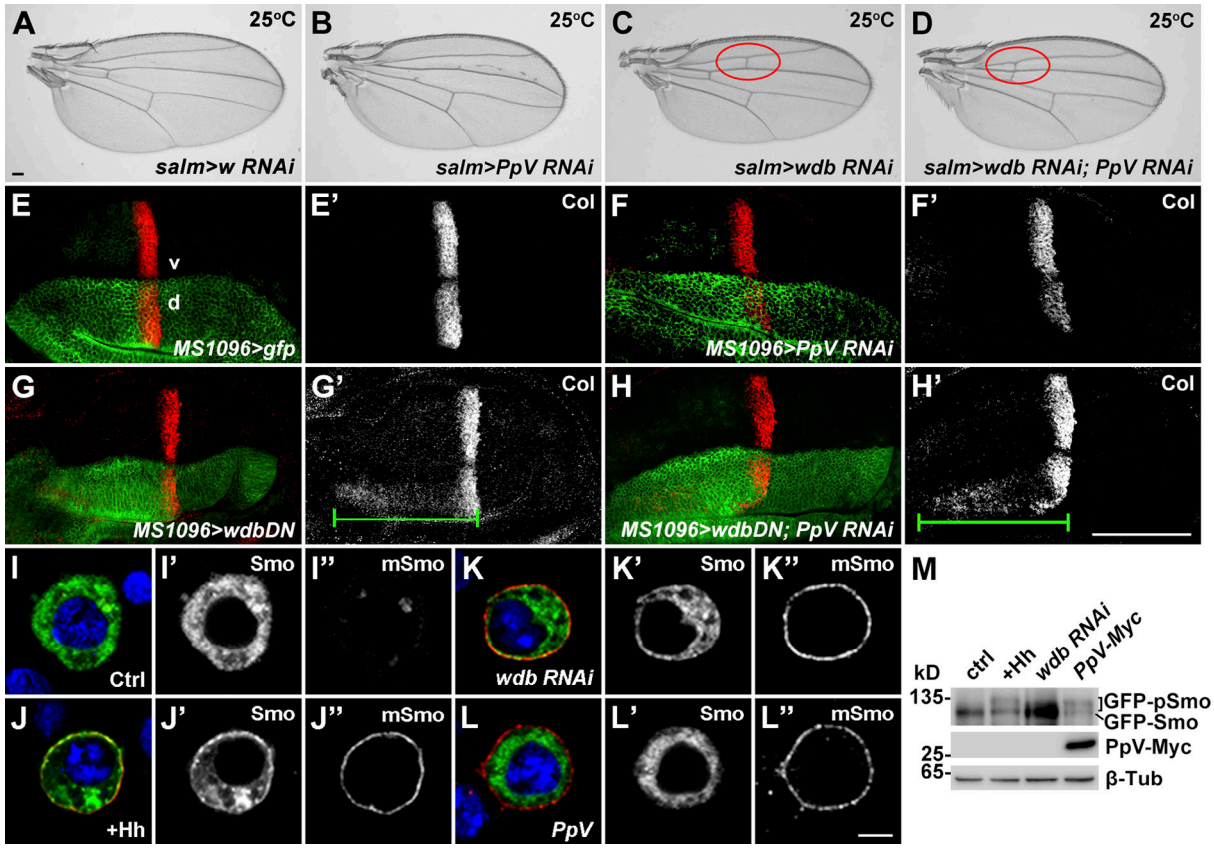


Figure 2. **PpV acts through Wdb to regulate Hh signaling. (A–D)** Co-expressing *wdb* RNAi and *PpV* RNAi by *salm*-Gal4 led to ectopic vein formation at anterior area of the wing (D), which resembles the phenotype of *wdb* RNAi alone (C), but not that of *PpV* RNAi (B). *White* (*W*) RNAi was used as a control for RNAi knockdown. Red circles mark the position where ectopic veins formed. **(E–H′)** Co-expressing $wdb^{DN}$ and *PpV* RNAi by *MS1096*-Gal4 in dorsal compartment of wing discs induced Col expression (i.e., high-level Hh signaling) to the anterior-most region (highlighted by a green line; H and H′), which resembled the phenotype of $wdb^{DN}$ alone (green line, G and G′), but not that of *PpV* RNAi (F and F′). Overexpressing *gfp* did not cause any obvious defect. **(I–L′′)** GFP-Smo (referred as Smo; green) localization was directly visualized by GFP fluorescence in S2 cells. Surface-localized GFP-Smo (referred as membrane Smo, mSmo; red) was detected by incubation with an antibody against Smo (20C6) without permeabilizing cells (I–I′′). Ectopic GFP-Smo was detected at cell surface upon treatment with Hh-conditioned medium (J–J′′), *wdb* dsRNA (K–K′′), or overexpressing *PpV* (L–L′′). **(M)** Phosphorylated forms of Smo (pSmo) were induced in GFP-Smo–expressing S2 cells treated with Hh-conditioned medium, *wdb* dsRNA, or overexpressing *PpV*. β-Tubulin, β-actin, or GAPDH served as loading controls for all experiments. Scale bars, A–H′, 100 µm; I–L′′, 5 µm. Ctrl, control; d, dorsal; v, ventral.

We found that the amount of endogenous Wdb was significantly increased in cell lysates extracted from hemizygous $PpV^{KO}$ larvae (Fig. 3 A). In WT wing disc epithelia, Wdb protein was predominantly localized to apical cytoplasm (Fig. 3, B and B′). However, increased amount of Wdb protein observed in *PpV* knockdown cells extended to basolateral cytoplasm (Fig. 3, C and C′). To further investigate how PpV regulates Wdb in vivo, we constructed a *heat-shock* (*hs*)-*wdb-HA* transgene where production of Wdb protein was controlled by a *hs* promoter. Reducing *PpV* expression in S2 cells by RNAi was still able to increase the amount of Wdb protein produced by the *hs* promoter (Fig. 3 D), while overexpressing *PpV* had an opposite effect (Fig. S2 A). Significantly, *hs*-Wdb protein accumulated in wing disc either following *PpV* knockdown (Fig. 3 F′) or in loss-of-function $PpV^{KO}$ mosaic clones (Fig. S2 B′), suggesting that the regulation of Wdb by PpV most likely takes place post-transcriptionally.

A common post-translational regulation mechanism is through protein turnover, via either proteasome- or lysosome-mediated degradation. Wdb protein produced in S2 cells had a relatively short half-life of around 3 h (Fig. S2 C). We found that the degradation of Wdb protein occurred through both proteasome- (Fig. S2 D) and lysosome-dependent pathways (Fig. S2 E), when nascent protein synthesis was blocked by cycloheximide. However, Wdb degradation induced by *PpV* overexpression was only inhibited when S2 cells were treated with proteasome inhibitor MG132, but not lysosome inhibitor chloroquine (CQ; Fig. 3 G), suggesting that the interaction between PpV and Wdb (Fig. 3, H and I) facilitates Wdb protein degradation in the proteasome. This conclusion was further supported by the observation that elevated *PpV* expression increased the degree of K48-linked poly-ubiquitination modification on Wdb (Fig. 3, J and K). Consistently, when all the lysine residues in Wdb protein, which may be potentially modified by ubiquitin (Ub) moiety, were mutated to arginine ($Wdb^{KR}$), the poly-ubiquitination modification on Wdb was significantly reduced (Fig. 3 L). As a result, $Wdb^{KR}$ protein became stabilized and was no longer subjected to regulation by PpV (Fig. 3 M; cf. Fig. S2 A).

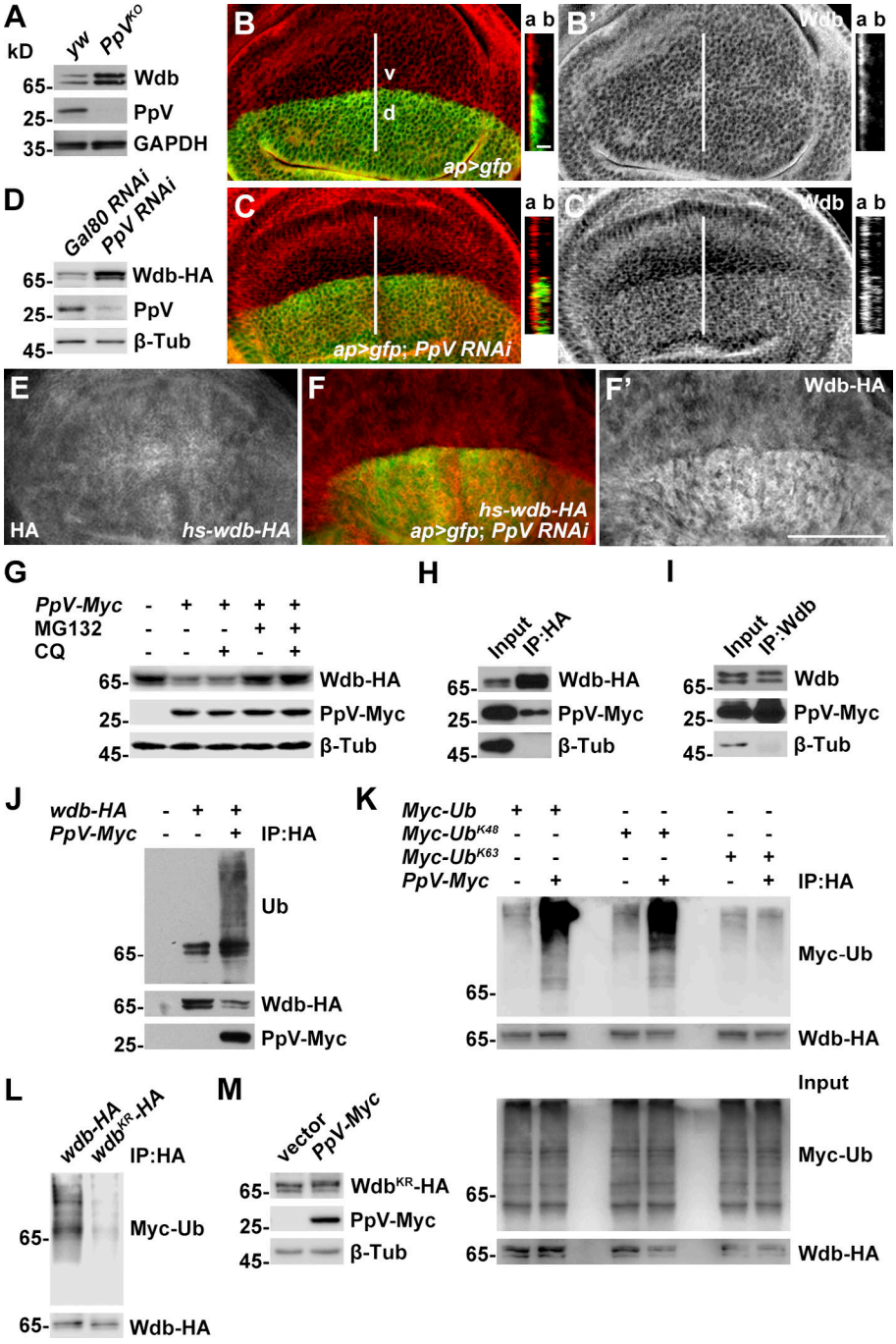


Figure 3. **PpV regulates Wdb protein turnover. (A)** *PpV* knockout resulted in increased amount of endogenous Wdb protein in hemizygous $PpV^{KO}$ larvae. **(B–C′)** In WT flies, Wdb protein uniformly located at the apical (a) cytoplasm of third instar wing disc cells (B and B′). *PpV* RNAi driven by *ap*-Gal4 in dorsal compartment of the wing disc led to increased amount of Wdb protein present in both apical and basal (b) cytoplasm (C and C′). Reconstituted optical cross-sections along the *z* axis were generated along the lines shown in B–C′. **(D–F′)** Exogenous Wdb-HA protein production controlled by a *hs* promoter (*hs*-Wdb-HA) was strongly elevated when *PpV* was knocked down in S2 cells as shown by immunoblotting (D) or when *PpV* RNAi was expressed by *ap*-Gal4 in dorsal compartment of the wing disc (F–F′). Note the uniform expression of *hs*-Wdb-HA protein in WT wing disc (E). **(G)** Degradation of PpV-induced exogenous Wdb protein (Wdb-HA) was inhibited mainly by MG132 in S2 cells. **(H and I)** Both exogenous Wdb-HA (H) and endogenous Wdb protein (I) coimmunoprecipitated with PpV-Myc in S2 cell lysates. **(J)** Overexpressing *PpV* in S2 cells increased poly-Ub modification of Wdb-HA. **(K)** Overexpressing *PpV* in S2 cells increased the level of K48 ($Ub^{K48}$) but not K63 ($Ub^{K63}$)-linked ubiquitination on Wdb protein. **(L)** Ub modification on Wdb protein was largely abolished when all the lysine residues in Wdb were mutated to arginine residues ($Wdb^{KR}$). **(M)** Overexpressing *PpV* did not alter the amount of $Wdb^{KR}$ protein in S2 cells. Scale bars, B–F′, 100 µm; reconstituted views in B–C′, 5 µm. d, dorsal; IP, immunoprecipitation; v, ventral.

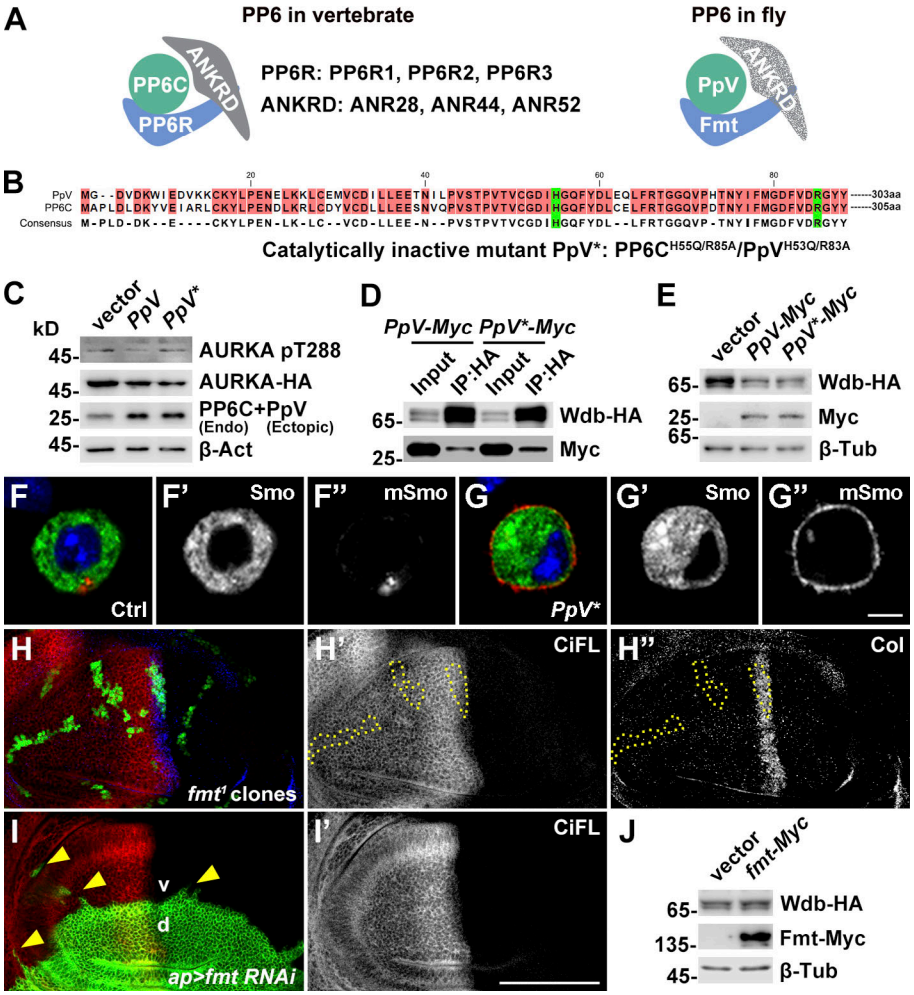


Figure 4. **PpV regulates Wdb independent of its phosphatase activity. (A)** The composition of both vertebrate and fly PP6 holoenzymes is shown. Note that the scaffolding ankyrin repeat domain–containing regulatory subunit (ANKRD) protein has not yet been identified in the fly complex. **(B)** Sequence alignment of catalytic domains of fly PpV and human PP6C. Conserved amino acids are shown in red. Amino acids essential for the phosphatase activity are highlighted in green. **(C)** PpV*, with two mutations (H53Q and R83A) in the catalytic domain, failed to dephosphorylate aurora A kinase (AURKA) at T288 in HEK293T cells treated with colchicine for 24 h. A PpV antibody we generated recognized both endogenous PP6C and overexpressed untagged PpV or PpV*. **(D and E)** PpV* had the same ability as WT PpV to interact with (D) and to induce Wdb degradation in S2 cells (E). **(F–G'')** Overexpressed PpV* had the same ability as WT PpV (cf. Fig. 2, L–L'') to induce GFP-Smo (Smo, green) accumulation at S2 cell surface (mSmo, red). **(H–H'')** There was no obvious change on CiFL stabilization or Col activation in loss-of-function *fmt*$^{1}$ wing disc clones, which were positively marked by GFP expression. Dotted lines mark *fmt*$^{1}$ clones. **(I and I')** *fmt* RNAi driven by *ap*-Gal4 in dorsal compartment of the wing disc induced cell protrusions (yellow arrowheads) extending to ventral compartment, a typical phenotype indicative of activated JNK signaling (Ma et al., 2017). However, *fmt* RNAi produced little effect on CiFL stabilization. **(J)** Overexpressing *fmt* was not able to alter the amount of *hs*-Wdb-HA protein in S2 cells. Scale bars, F–G'', 5 µm; H–I', 100 µm. d, dorsal; IP, immunoprecipitation; mSmo, membrane Smo; v, ventral.

## PpV facilitates Wdb protein degradation independent of its phosphatase activity

In vertebrates, the conserved PP6 heterotrimeric holoenzyme is composed of catalytic subunit (PP6C), one of three scaffolding ankyrin repeat domain–containing regulatory subunits and one of three Sit4-associated proteins domain–containing regulatory subunits (PP6R; Fig. 4 A; Ohama, 2019). Over the past decade, PP6C/PpV and its regulatory subunits have been reported to regulate several substrates in diverse cellular processes (Kajino et al., 2006; Mi et al., 2009; Zeng et al., 2010; Hosing et al., 2012; Ertych et al., 2016; Ma et al., 2017; Liu et al., 2019, 2020). Recently, phosphoproteomics in mammalian cells identified >200 potential PP6 substrates, implying that PP6 functions in a broad range of biological processes (Rusin et al., 2015).

Given the fact that PpV is the catalytic subunit of PP6 holoenzyme in *Drosophila* (Fig. 4 A), we reasoned that PpV may rely on its phosphatase activity to modulate Wdb protein stability. Endogenous as well as overexpressed Wdb protein in S2 cells migrated as a doublet with an apparent molecular mass of ∼65 kD. Upon treatment with calf intestine phosphatase, both bands migrated faster when compared with untreated lysates (Fig. S3, A and B), suggesting that both forms of Wdb were phosphorylated, an observation also supported by enrichment of endogenous phospho-Wdb protein (Fig. S3 C). However, to our surprise, manipulating the expression of *PpV* in *PpV* knockout

larvae (Fig. 3 A) or in wing discs expressing *PpV* RNAi (Fig. 3 D) or in S2 cells overexpressing *PpV* (Fig. S2 A) had little effect on the electrophoretic migration of endogenous or ectopically produced Wdb protein, raising a likely possibility that PpV-regulated Wdb protein abundance is independent of its phosphatase activity.

To test this hypothesis directly, we generated a phosphatase inactive form of *PpV* (*PpV**; Fig. 4 B). When introduced into a WT background containing an active allele, PpV* lost its phosphatase activity to dephosphorylate Aurora A kinase, a known PP6 substrate (Fig. 4 C; Zeng et al., 2010). We found that PpV* retained the ability to interact with (Fig. 4 D) and to reduce protein abundance of Wdb in S2 cells (Fig. 4 E). Furthermore, overexpressed *PpV** induced hyper-phosphorylation and translocation of Smo from the cytosol to the plasma membrane (Fig. 4, F–G′′). The phosphatase activity of PP6 holoenzyme requires the coordination of its obligate Sit4-associated proteins domain–containing regulatory subunit. *fiery mountain* (*fmt*) encodes the sole regulatory subunit of the fly PP6 (Fig. 4 A; Ma et al., 2017). When *fmt* function was compromised in wing discs either in *fmt* loss-of-function clones or by RNAi, however, there was no obvious change in Hh target expression (Fig. 4, H–I′; and Fig. S3, D and D′). These results were consistent with the observation that *fmt* overexpression was not able to reduce Wdb protein abundance in S2 cells (Fig. 4 J). Taken together, the above data indicate that the PpV regulation of Wdb does not rely on its phosphatase activity.

### PpV facilitates Wdb degradation by interference with the PP2A complex assembly

Since the phosphatase activity of PpV was not required for regulation of Wdb stability, we sought alternative mechanisms. It is known that the assembly of PP2A heterotrimeric complex enhances the stability of individual constituent subunits (Li et al., 2002; Silverstein et al., 2002; Janssens et al., 2003; Strack et al., 2004; Chen et al., 2005). Indeed, when Microtubule star (Mts), the catalytic subunit of PP2A (PP2Ac), was removed from the PP2A holoenzyme in S2 cells by RNAi, the amount of endogenous Wdb protein present in cell lysates was significantly reduced (Fig. 5 A). This was likely a consequence of shorter half-life of Wdb in cells treated with *mts* RNAi when compared with the control *Gal80* RNAi (Fig. 5 B). Similarly, the half-life of mutant Wdb protein was reduced (Fig. 5 C) when its binding sites for Mts (Xu et al., 2006) were removed (Fig. 5 D). Concurrently, increased degree of Wdb ubiquitination was observed (Fig. 5 E). As PpV and Mts serve as respective catalytic subunits of PP6 and PP2A holoenzymes, which are two structurally closely related phosphatases (Kong et al., 2009), the above results led us to hypothesize that PpV may compete with Mts for assembly of PP2A holoenzyme, resulting in destabilization of Wdb. To directly test this hypothesis, we examined in S2 cells the interaction between Wdb and Mts following alteration of PpV expression. We found that ectopic *PpV* expression significantly decreased the amount of Mts coimmunoprecipitating with Wdb protein (Fig. 5 F). More strikingly, this competition between Mts and PpV for Wdb association was dose dependent (Fig. 5, G–I). Taken together, our results uncover a new type of phosphatase regulation in which PpV facilitates Wdb protein degradation through its ability to compete with Mts, thus preventing Wdb from forming a functional stable Wdb-PP2A complex (Fig. 5 J).

### The expression of *PpV* correlates with graded Hh signaling

Having established how PpV regulates Wdb activity, we next examined the relationship between PpV and graded Hh signaling. We found that both the activity (Fig. 6 A) and the protein abundance of Wdb (Fig. 6, B and D–D′′) were negatively regulated by Hh signaling. We further found this regulation to be post-transcriptional, as altering Hh signaling in the wing disc had little effect on *wdb* transcription (Fig. 6, C and E–G′′). Since *wdb* acts epistatically to *PpV*, we therefore entertained the possibility that Hh signaling may directly regulate *PpV* expression to control Wdb-PP2A activity. Thus, we generated an antibody specific for endogenous PpV protein (Fig. 3, A and D; and Fig. S4 A′). Immunofluorescence analyses revealed an intriguing PpV expression pattern (Fig. 7 G′′): it accumulated at a higher level in anterior compartment of the wing disc, with the exception of the posterior-most cells of the anterior compartment, where PpV protein accumulation declined sharply (Fig. 7 B). These posterior-most cells (shown in purple in Fig. 7, B and B′) also expressed a higher level of Smo (Denef et al., 2000). We reasoned that these cells must receive the highest concentration of Hh morophogen, as they partially overlap with the cells whose CiFL was converted to a labile form of active Ci (CiA; i.e., lower-level), in response to high-level Hh signaling (shown in violet and purple in Fig. 7, B and B′). Taken together, the expression pattern of PpV led us to propose that Hh signaling activates PpV expression, except for cells receiving the highest levels of Hh signaling, which represses its expression.

To test this hypothesis, we manipulated Hh signaling in wing discs and examined its effect on the level of endogenous PpV protein. Consistent with our hypothesis, when *ci* was overexpressed along the anterior–posterior (a-p) boundary, elevated PpV expression was observed (Fig. S4, B and B′). This result also holds in $ptc^{S2}$ homozygous mutant clones: PpV expression was significantly up-regulated in clones away from the a-p boundary (Fig. 7, C–C1′′′). Furthermore, when the a-p boundary displaying the highest signaling (i.e., with labile CiA) was expanded by overexpressing *ptc* RNAi in the dorsal compartment of the wing disc (Fig. 7 D), PpV expression was reduced accordingly (arrows in Fig. 7, E–E′′). As the cells receiving the highest Hh signaling activate *engrailed* (*en*), which can serve as a repressor for anteriorly expressed genes required for wing development, such as *ptc* and *dpp* (Guillén et al., 1995; Sanicola et al., 1995; Tabata et al., 1995), we asked whether En contributed to the repression of *PpV*. Indeed, knocking down *en* successfully restored the expression of *PpV* (arrow in Fig. 7 F′′) in expanded a-p boundary, where cells exhibited highest Hh signaling activity resulted from *ptc* RNAi (Fig. 7 F′′′). Taken together, the above results demonstrate that PpV expression indeed responds differentially to graded Hh signaling.

### *PpV* is a genuine Hh transcriptional target

As the expression of PpV protein is differentially regulated by Hh signaling, we then asked if this regulation takes place at

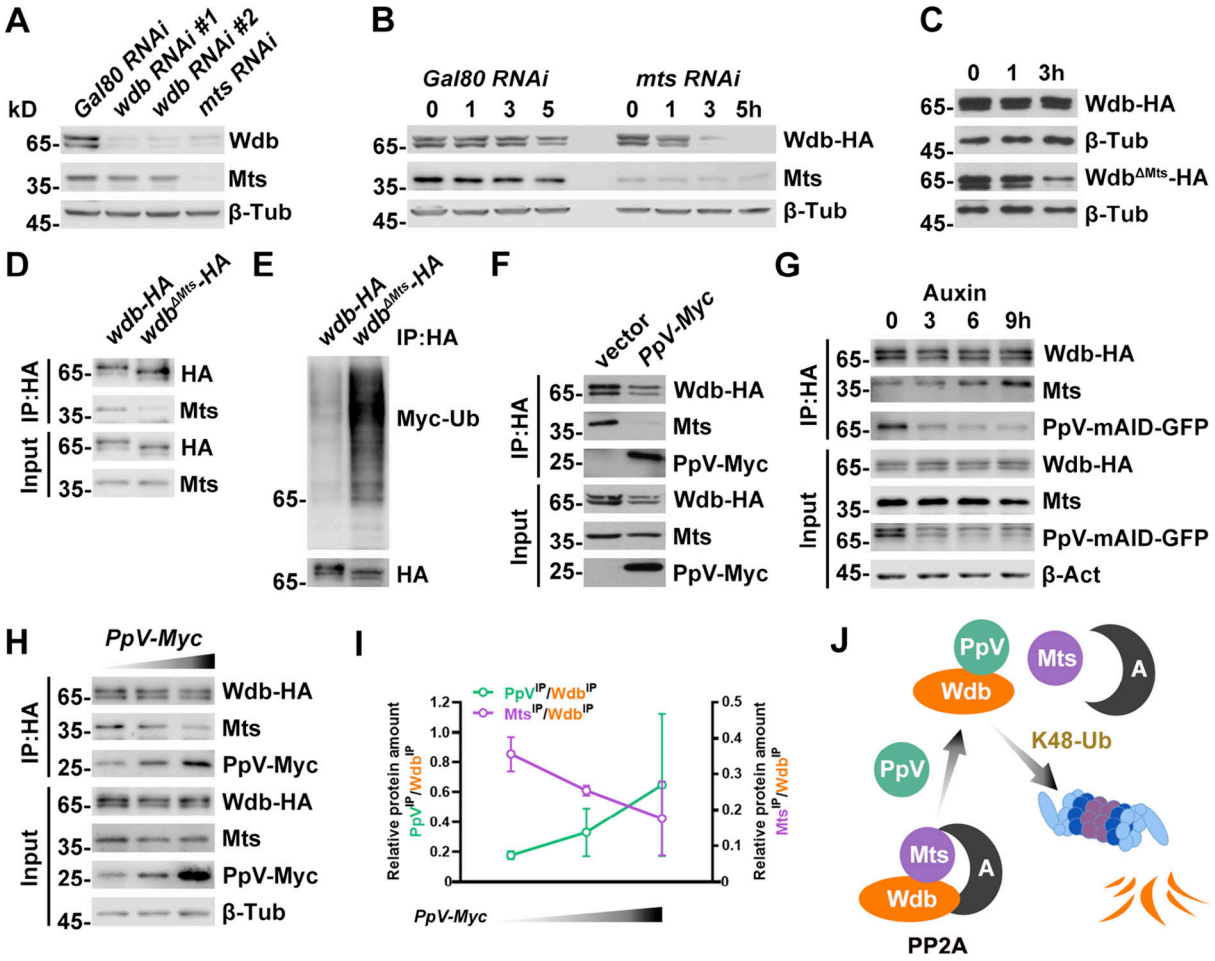


Figure 5. **PpV interferes with the PP2A complex assembly. (A)** Knocking down *mts* in S2 cells resulted in reduced amount of endogenous Wdb protein. **(B)** Knocking down *mts* in S2 cells promoted degradation of Wdb protein. **(C)** $Wdb^{\Delta Mts}$ protein, whose binding motif with the PP2A catalytic subunit Mts was removed, was less stable than WT Wdb. **(D)** $Wdb^{\Delta Mts}$ protein was not able to efficiently interact with Mts as compared with that of WT Wdb. **(E)** Poly-Ub modification of $Wdb^{\Delta Mts}$ protein was increased. **(F)** Overexpressing *PpV* in S2 cells significantly reduced the amount of endogenous Mts coimmunoprecipitated with Wdb. **(G)** When PpV containing a minimal auxin-inducible degron (mAID) was quickly degraded, a process mediated by auxin primed formation of OsTIR1-SCF (Skp1–Cul1–F box) E3 ligase complex, the amount of endogenous Mts that coimmunoprecipitated with Wdb was increased in a dose-dependent manner. **(H and I)** Increasing amounts of overexpressed *PpV* competed with endogenous Mts for coimmunoprecipitation with Wdb in a dose-dependent manner (H). Normalized amount of PpV or Mts protein in association with Wdb after coimmunoprecipitation was shown (I). The amounts of Wdb, Mts, or PpV were determined by ImageJ based on mean pixel intensity of each band shown in the blots. Relative amount of PpV or Mts protein associated with Wdb was measured by calculating pixel intensity ratio between PpV or Mts and relevant Wdb bands in each lane. The dataset of $PpV^{IP}/Wdb^{IP}$ was plotted on the y axis to the left side, while $Mts^{IP}/Wdb^{IP}$ was plotted to the right side. Standard deviations are shown ($n$ = 3). **(J)** Wdb-PP2A holoenzyme is composed of scaffolding A subunit PP2A-29B, regulatory B subunit Wdb and catalytic C subunit Mts The association between PpV, the catalytic subunit of PP6, and Wdb leads to disassembly of Wdb-PP2A holoenzyme. Consequently, Wdb protein undergoes K48-linked poly-ubiquitination, which facilitates its subsequent degradation in proteasome. IP, immunoprecipitation.

transcriptional level. We performed in situ hybridization in WT wing discs to reveal the transcription profile of *PpV*. Similar to the results of PpV antibody staining, *PpV* transcript was expressed at a higher level in anterior compartment of the wing disc (Fig. 8 B′). Furthermore, mRNA expression pattern altered similarly to protein expression pattern when Hh signaling activity was manipulated (Fig. S5, B and C), highly consistent with *PpV* serving as a direct transcriptional target of Hh signaling.

Most Hh targets rely on the presence of clustered Ci/Gli consensus sites for binding of Hh signaling transcription factors (Gurdziel et al., 2015). Upon scanning the *PpV* locus using the Genomatix MatInspector algorithm (http://www.genomatix.de), we identified two clusters of putative Ci/Gli binding sites, as well as three scattered sites spanning a 4-kb region upstream of the *PpV* transcription start site (*PpV* 5′; Fig. 8 A and Fig. S5 A). To determine functional importance of these putative binding sites, we first constructed a GFP reporter transgene under control of the *PpV* 5′ (Fig. 8 A). The expression pattern of the resulting *PpV* 5′-GFP reporter correlated well with that of the *PpV* mRNA (Fig. 8 C′). More importantly, the *PpV* 5′-GFP reporter responded sufficiently to altered Hh signaling (Fig. S5, D–E′′). Having shown the importance of this regulatory region in the *PpV* locus for *PpV* transcription, we then examined whether putative Ci/Gli binding sites present in this region are capable of mediating direct interactions with the fly Hh signaling transcription factor Ci. The DNA-binding zinc-finger

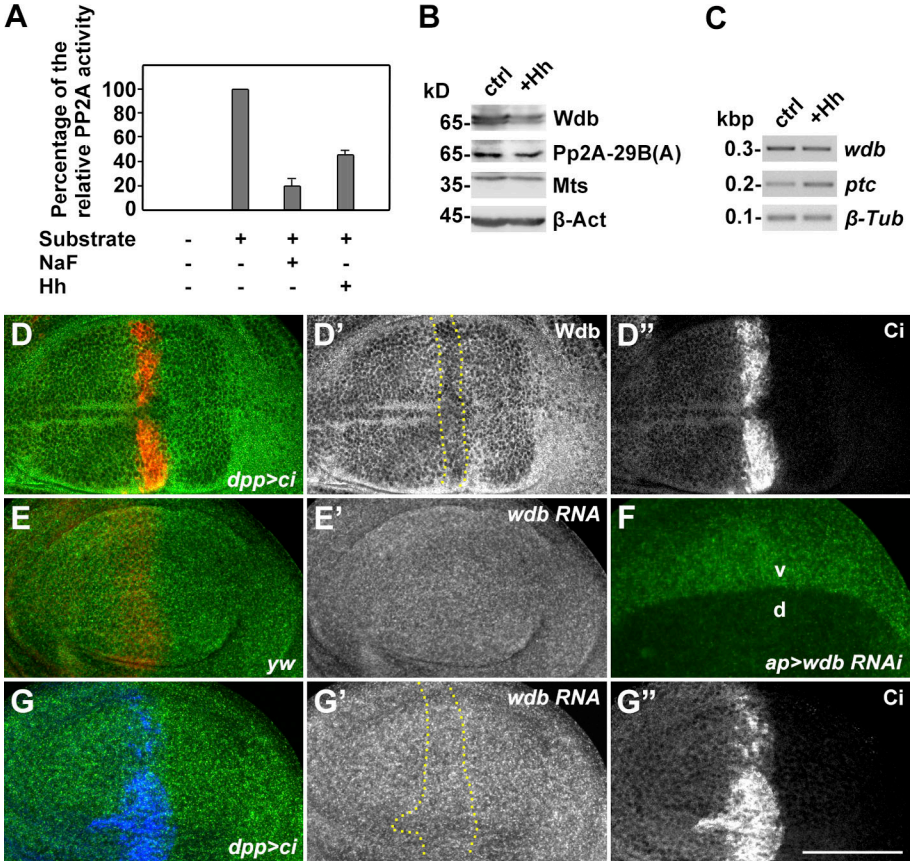


Figure 6. **Wdb-PP2A is regulated by Hh signaling at the post-transcriptional level. (A)** Increased Hh signaling reduced PP2A activity. Normalized PP2A activity of wing discs expressing *gfp* or *hhN* by *MS1096*-Gal4 was determined. The reading from wing discs expressing *gfp* was set as 100% of the PP2A activity (basal activity). 50 mM phosphatase inhibitor NaF was sufficient to inhibit the PP2A activity. Wing discs expressing *hhN* exhibited ∼40% ($P < 0.001$) of the basal PP2A activity. Standard deviations are shown ($n = 3$). **(B)** The effect of Hh signaling in Wdb-PP2A holoenzyme. The amount of endogenous regulatory subunit Wdb protein, but not catalytic subunit Mts or scaffolding subunit PP2A-29B, was reduced in wing discs expressing *hhN* (+Hh) compared with *gfp* (ctrl), driven by *MS1096*-Gal4. **(C)** The effect of Hh signaling in *wdb* transcription. *wdb* mRNA analyzed by RT-PCR was not altered in wing discs expressing *hhN* (+Hh) compared with *gfp* (ctrl), driven by *MS1096*-Gal4. In contrast, *ptc* mRNA, which is a direct Hh target, was increased. **(D–D′′)** Overexpressing *ci* along the a-p boundary of wing disc by *dpp*-Gal4 reduced the amount of Wdb protein. Dotted lines mark the expression domain of *dpp*-Gal4 in D′ and G′. **(E and F)** *wdb* was uniformly expressed in wing discs as revealed by in situ hybridization (E–E′). Knocking down *wdb* in the dorsal (d) compartment of wing disc by RNAi specifically reduced *wdb* expression (F), indicating the effectiveness of the *wdb* RNA probe. **(G–G′′)** Overexpressing *ci* by *dpp*-Gal4 did not alter *wdb* transcription. Scale bar, 100 µm. d, dorsal; v, ventral.

domain of the Ci protein (Ci ZnF), which binds efficiently to verified Ci binding sites (*ptc*-5) in the *ptc* locus (Fig. 8 D; Gurdziel et al., 2015), was purified and used in the electrophoretic mobility shift assay. Our DNA binding and competition assays (shown in Fig. 8 D) showed direct and sequence-specific binding of Ci ZnF to all five consensus sites, supporting a potential role of these Ci/Gli binding sites in the *PpV* 5′ in mediating the effect of graded Hh signaling on *PpV* expression.

To conclusively demonstrate the requirement of the Ci/Gli binding sites in the *PpV* 5′ on *PpV* expression in vivo, we generated $PpV^{5'KO}$, a *PpV* regulatory sequence deletion mutant in which the *PpV* 5′ containing all five Ci/Gli binding sites was removed (Fig. 8 A). As predicted, PpV no longer accumulated at the higher level in the anterior compartment of hemizygous $PpV^{5'KO}$ wing discs (Fig. 8 E′; cf. Fig. 7 A′′). Consequently, $PpV^{5'KO}$ also lost its ability to respond to heightened Hh signaling (Fig. 8 F′; cf. Fig. S4 B′). Taken together, our results provide sufficient evidence for *PpV* as a bona fide Hh signaling target whose transcription is maintained by graded Hh signaling.

## Discussion

Taking advantage of fly genetics, we uncover a noncanonical role of protein phosphatase PpV in transducing high-level Hh signaling. The identification of Wdb, the regulatory subunit of PP2A, as a PpV target provides a mechanistic basis for PpV regulation of Hh signaling. PpV interferes with assembly of the Wdb-PP2A complex, in turn facilitating Wdb ubiquitination and its ultimate degradation in proteasome. Importantly, *PpV* itself is a bona fide transcriptional target of Hh signaling, forming a negative feedback loop between two closely related phosphatases to maintain homeostatic Hh signaling.

### PpV acts as a graded Hh signaling sensor in the feedback control of Hh signaling homeostasis

The conversion of extracellular Hh morphogen gradient into distinct transcriptional outputs relies on graded Smo phosphorylation. This stereotypical Smo phosphorylation profile is maintained by coordinated actions of kinases and phosphatases.

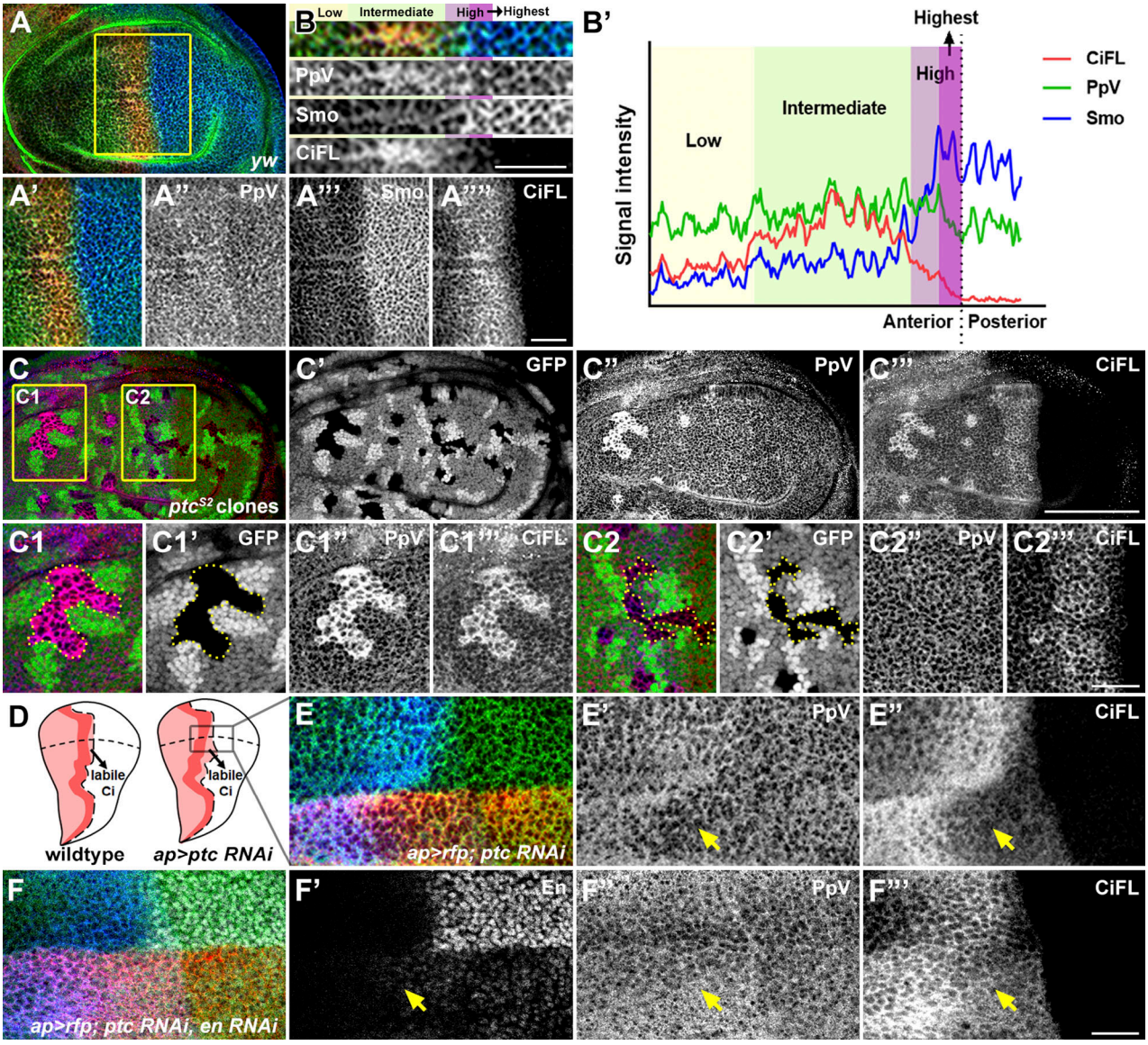


Figure 7. **PpV is regulated by the Hh signaling. (A–A′′′′)** Shown are expression patterns of PpV, CiFL, and Smo in a WT wing disc. Enlarged boxed area is shown in A′–A′′′′. **(B and B′)** The expression of PpV, CiFL, and Smo shown in B was analyzed with ImageJ. The horizontal axis represents the a-p orientation (anterior to the left and posterior to the right). Dashed line indicates the a-p boundary. Anterior compartment cells responding to low, intermediate, and high levels of Hh signaling are shown in yellow, green, and violet, respectively. Cells responding to the highest Hh signaling are shown in purple. A higher amount of PpV protein was found in anterior cells, with the exception of the posterior-most cells in anterior compartment (highlighted in purple), where PpV protein accumulation declined sharply. **(C–C2′′′)** Increased amount of PpV protein was found in loss-of-function *ptc*$^{S2}$ somatic clones (marked by the absence of GFP) away from (i.e., low-to-intermediate Hh signaling; C1–C1′′′) but not abutting the a-p boundary (i.e., high-level signaling; C2–C2′′′). Enlarged boxed areas (C) are shown (C1–C1′′′ and C2–C2′′′). Both PpV expression (C1′′) and CiFL stabilization (C1′′′) were increased in *ptc*$^{S2}$ clones away from the a-p boundary. In clones abutting the boundary, PpV expression was not altered, but the amount of CiFL was reduced, probably due to conversion of CiFL to labile CiA in response to high-level Hh signaling. Dotted lines mark *ptc*$^{S2}$ clones (C1, C1′, C2, and C2′). **(D)** Schematic drawing of a WT wing disc and a wing disc expressing *ptc* RNAi. At the a-p boundary of a WT wing disc, CiFL was converted to an active but labile form (i.e., lower level) of CiA. Upon overexpressing *ptc* RNAi by *ap*-Gal4 in dorsal compartment, the a-p boundary displaying high levels of Hh signaling (i.e., with labile Ci) was expanded. **(E–E′′)** PpV protein production was reduced in expanded region (yellow arrows) labeled by labile CiFL when *ptc RNAi* was expressed by *ap*-Gal4 in a wing disc. **(F–F′′′)** PpV protein production was restored in *ptc RNAi*-induced expanded region (yellow arrows) labeled by labile CiFL when *en RNAi* was expressed by *ap*-Gal4 in a wing disc. Scale bars, A and C–C′′′, 100 µm; A′–A′′′′, B, C1–C2′′′, and E–F′′′, 25 µm.

A key unresolved question is whether and how the activities of these kinases and phosphatases are regulated when Hh signaling fluctuates. In our study, we showed that Wdb-PP2A activity negatively correlates with Hh signaling, providing a mechanism for ensuring a sufficient amount of highly phosphorylated Smo species for transducing high-level Hh signaling. However, the regulation of Wdb by Hh is indirect. Here, through an unbiased genetic screen, we identify PpV as the protein that directly responds to the Hh gradient. Importantly, PpV also serves as a direct Hh signaling sensor that coordinates Wdb-PP2A activity

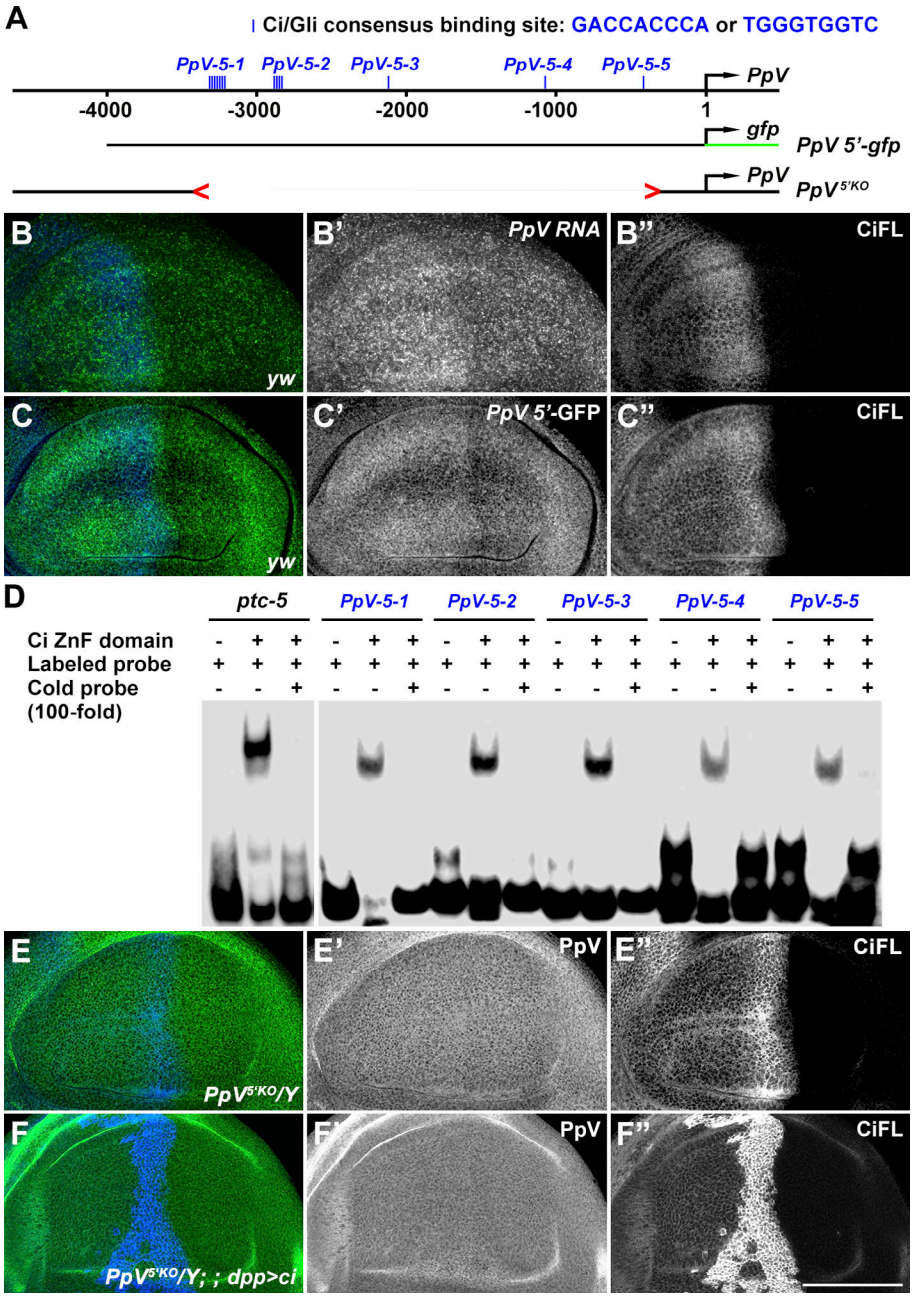


Figure 8. ***PpV* serves as a bona fide Hh transcriptional target. (A)** Multiple putative Ci/Gli consensus binding sites, including two clusters (*PpV-5-1* and *PpV-5-2*) and three scattered sites (*PpV-5-3*, *PpV-5-4* and *PpV-5-5*), are found at 5′ regulatory sequence of the *PpV* locus. A 4 kb region upstream of *PpV* transcription start site (*PpV 5′*) encompassing all the putative Ci/Gli binding sites was cloned into a GFP reporter to examine the effect of Hh signaling on *PpV* transcription. The sequence containing putative Ci/Gli binding sites was deleted in $PpV^{5'KO}$ mutant flies. **(B–B′′)** *PpV* transcript was expressed at a higher level at anterior compartment of a wing disc as revealed by in situ hybridization. **(C–C′′)** The *PpV 5′*-GFP reporter was expressed at a higher level at anterior compartment of a wing disc. CiFL expression marks the a-p boundary (B–C′′). **(D)** As analyzed by electrophoretic mobility shift assay, biotin-labeled DNA probe *ptc-5*, which contains previously verified Ci binding sites, as well as the five putative Ci/Gli binding sites present at the 5′ regulatory sequence of the *PpV* locus, were bound efficiently by GST-tagged Ci ZnF purified from bacteria. The Ci ZnF binding to each consensus site was abolished when an excess amount (100-fold) of unlabeled cold competitor probe was added. **(E–E′′)** PpV protein no longer accumulated at a higher level in the anterior compartment of a hemizygous $PpV^{5'KO}$ wing disc. **(F–F′′)** Overexpressing *ci* on the a-p boundary of a wing disc by *dpp*-Gal4 was no longer able to promote the production of PpV protein in $PpV^{5'KO}$ mutant (cf. Fig. S4 B′). Scale bar, 100 µm.

and graded Smo phosphorylation. When *PpV* expression is reduced or Wdb-PP2A activity is enhanced in the developing wing, the Smo phosphorylation profile is shifted from the highly phosphorylated Smo state toward moderate and basal levels of Smo phosphorylation, resulting in elevated low to intermediate levels of Hh signaling at the expense of high-level signaling. By acting both as a sensor and target of Hh signaling, and participating in feedback regulatory loops, PpV contributes to the robustness and reliability of Hh signaling.

As the *PpV* locus contains clustered, functional Ci binding sites, Hh signaling is sufficient to activate *PpV* transcription in the anterior compartment of the wing disc. However, we noticed that the expression level of *PpV* is lower in anterior cells immediately adjacent to the a-p boundary. These cells likely exhibit the highest Hh activity, as they maintain higher levels of Smo and coincide with the posterior half of the CiA-expressing region. Consistently, the reduced *PpV* expression becomes even more apparent when Hh signaling is hyper-activated abutting the a-p boundary. Therefore, in cells with excess Hh signaling, it is necessary to reduce the PpV level, which primes cells for heightened Wdb-PP2A activity to prevent Smo from hyper-phosphorylation. Hence, Hh signaling homeostasis is maintained. How cells sense excess Hh morphogen concentration to tune down *PpV* transcription is not known. Nevertheless, observation of the same phenomenon in wing discs expressing a *PpV 5′-GFP* reporter suggests that the control elements differentially regulating *PpV* expression most likely reside in the 5′ regulatory region. In addition to the Ci consensus sites, an array of binding sites for other transcription factors, including En/EN1, are present (Fig. S5 A). Intriguingly, En can serve as a repressor for anteriorly expressed genes required for wing development, such as *ptc* and *dpp* (Guillén et al., 1995; Sanicola et al., 1995; Tabata et al., 1995). As En expression extends to anterior cells immediately adjacent to the a-p boundary, we believe that combinatory activities of Ci and En may potentially facilitate dynamic regulation of *PpV* expression in response to differential Hh signaling. Thus, it would be interesting to investigate how En activity at the a-p boundary reduces *PpV* expression.

Coordinated cell signaling is required for development and adult homeostasis. Feedback and feed-forward mechanisms are used to robustly define the behavior of cell signaling, while negative feedback loops are important for homeostatic maintenance of signaling activity. Negative regulators are the key to a feedback regulatory network, as they often contribute sensitivity and dynamic regulation, rather than simply terminating the signal transduction (Kholodenko, 2006; Alon, 2007; Brandman and Meyer, 2008; Lemmon et al., 2016). The most well-known negative feedback loop in Hh signaling is mediated by the Hh receptor Ptc, which is itself a transcriptional target of Hh signaling, shutting down the signal activation through Hh sequestration (Chen and Struhl, 1996; Strutt et al., 2001; Torroja et al., 2004). Even though additional negative regulators have been identified for homeostatic control of the transcriptional factor Ci or essential activator Smo through ubiquination-mediated degradation pathway and kinase/phosphatase cycles (Briscoe and Thérond, 2013; Lee et al., 2016; Pak and Segal, 2016), very few regulators respond directly to graded Hh signaling at the transcriptional level (Atwood et al., 2013). The identification of *PpV* as a graded Hh signaling sensor provides an innovative feedback regulatory mechanism, with enhanced self-regulatory capacity to buffer fluctuations in Hh morphogen gradient during development.

### PpV/PP6C modulates PP2A holoenzyme assembly and protein homeostasis

Increasing evidence demonstrates that PP2A dysregulation is a repeated theme in many diseases, including neurodegenerative disorders, cardiovascular diseases, and cancer (O'Connor et al., 2018). Various endogenous and exogenous inhibitors of PP2A have been shown to contribute significantly to the development of PP2A-related diseases, making them valuable therapeutic targets (Sangodkar et al., 2016; O'Connor et al., 2018). The most prominent mechanism used to inhibit the phosphatase activity in cancer cells is competitive binding of inhibitors to different PP2A subunits, thereby preventing the interaction of the phosphatase active site with substrate proteins (Junttila et al., 2007). Indeed, PP2A reactivation drugs specifically targeting these inhibitors, including cancerous inhibitor of PP2A (CIP2A) and SE translocation oncoprotein (SET), have been successfully developed (Sangodkar et al., 2016; O'Connor et al., 2018).

Our study uncovers a new inhibitory mechanism by which an endogenous catalytic subunit of a PP2A family phosphatase (i.e., PP6C), which is structurally closely related to PP2Ac, competitively blocks the PP2A holoenzyme assembly. Based on our study, we suspect that PpV/PP6C may have a higher affinity for the regulatory subunit Wdb than that of Mts/PP2Ac. Upon PpV binding, Wdb may allosterically change its conformation that interferes with its ability to interact with Mts/PP2Ac. Although the resulting PpV-Wdb complex may be active, its highly unstable nature might prevent it from functioning on PP2A substrates. Our finding highlights a possible use of PP6 as an alternative therapeutic strategy for PP2A activation. Recent studies reveal that allosteric small molecule activators of PP2A specifically stabilize the PPP2R5A (B56α)- and PPP2R2A (B55α)-PP2A holoenzymes in a fully assembled active state to dephosphorylate selective substrates, such as c-Myc (Leonard et al., 2020; Morita et al., 2020), while phenothiazine analogues improved heterocyclic PP2A activators activate PP2A complexes that contain only the PPP2R5E (B56ε) regulatory subunit (Morita et al., 2020). As there are more than 26 regulatory B subunits known to complex with PP2Ac to confer its substrate specificity, identifying the PP2A regulatory subunit whose stability is regulated by PP6 would aid the development of novel therapeutic targets.

## Materials and methods

### Fly genetics

Fly cultures and crosses were performed according to standard procedures. *Drosophila* stocks were ordered from stock centers or obtained from other laboratories and are listed as follows: *ap*-Gal4 (Bloomington *Drosophila* Stock Center [BDSC]; 3041), $ci^{cell}$ (BDSC; 4343), *dpp*-Gal4 (BDSC; 1553), *dpp-lacZ* (BDSC; 8411), $fmt^{1}$ (BDSC; 82141; Ma et al., 2017), $fmt^{f02530}$ (BDSC; 18559), *hs-*$Flp^{122}$*; Act>y+>Gal4, UAS-nls::gfp; Tub-Gal80, FRT79E* (a gift of J. Pastor-Pareja, Tsinghua University, Beijing, China), *hs-*$Flp^{122}$*; FRT42D, Ubi-gfp* (a gift of J.E. Treisman, New York University, New York, NY), *MS1096*-Gal4 (BDSC; 8860), $ptc^{S2}$ (BDSC; 6332), *salm*-Gal4 (BDSC; 5818), UAS-*ci-HA* (Domínguez et al., 1996), UAS-*ci RNAi* (BDSC; 28984), UAS-*en RNAi* (Vienna *Drosophila* RNAi Center [VDRC]; 35697; Dietzl et al., 2007), UAS-*fmt RNAi* (VDRC; 16005), UAS–N-terminal of Hh protein, an active form of Hh [*hhN*]; Porter et al., 1995), UAS-*mCD8::gfp* (BDSC; 5130), UAS-*ptcB1* (BDSC; 5817; Johnson et al., 1995), UAS-*ptc RNAi* (BDSC;

28795), UAS-*PpV RNAi* (VDRC; 101997; and VDRC; 31690), UAS-*puc* (Ma et al., 2017), UAS-*wdbDN* (Hannus et al., 2002), UAS-*wdb RNAi* (VDRC; 27470), UAS-*w RNAi* (TsingHua Fly Center; HU0583) and *yw* (BDSC; 1495). Detailed genetic crosses shown in each figure are listed in Table S1.

*PpV*$^{KO}$ flies were generated through homologous recombination with donor plasmid *pTV-Cherry* obtained from J.-P. Vincent (The Francis Crick Institute, London, UK). Details were performed according to procedures previously described (Baena-Lopez et al., 2013). Briefly, ~3 kb genomic sequence flanking the *PpV* coding sequence was cloned into *pTV-Cherry* as homology arms to generate donor flies. After crossing to flies expressing FLP; I-SceI and then *Ub*-Gal4(*3xP3-GFP*), red-eyed F2 homologous recombinant flies were collected and confirmed by PCR. *PpV*$^{5'KO}$ flies were generated by CRISPR/Cas9-mediated homologous recombination (Port et al., 2014). *hs-wdb-HA* and *PpV 5′-gfp* reporter transgenic flies were generated by *P*-element–mediated germline transformation. Primers used for generating fly transformation constructs are listed in Table S2.

### Immunofluorescence staining, in situ hybridization, and adult fly wing imaging

For conventional immunofluorescence staining, wing discs dissected from third instar larvae were fixed in 4% paraformaldehyde, blocked in 0.2% BSA for 1 h, and incubated overnight at 4°C with primary antibodies: mouse anti-β-galactosidase (1:200; Developmental Studies Hybridoma Bank [DSHB]; 40-1a), rat anti-Ci full-length (1:10; DSHB; 2A1), rat anti-Col (1:2,000; generated in this study), rabbit anti-GFP (1:1,000; Thermo Fisher Scientific; A-11122), mouse anti-En (1:500; DSHB; 4D9), mouse anti-HA (1:1,000; Cell Signaling Technology [CST]; 2367S), rabbit anti-PpV (1:100; generated in this study), mouse anti-Smo (1:20; DSHB; 20C6), and guinea pig anti-Wdb (1:500; a gift of A. Sehgal, University of Pennsylvania, Philadelphia, PA). For cell staining, *Drosophila* Schneider S2 cells (American Type Culture Collection [ATCC]; CRL-1963) grown on coverslips were fixed with 4% paraformaldehyde before direct visualization. The coverslips seeded with S2 cells were precoated with poly-L-lysine (Sigma-Aldrich). To visualize transiently transfected S2 cells expressing *gfp-smo*, we used mouse anti-Smo (DSHB; 20C6) antibody to stain fixed but not permeabilized cells. Under this condition, 20C6 was able to detect GFP-Smo on the surface of S2 cells. The wing discs or cells were then incubated with goat anti-mouse/rabbit/rat/guinea pig Alexa Fluor–conjugated secondary antibodies (1:400; Thermo Fisher Scientific; A-11001, A-11004, A-11006, A-11008, A-11011, A-11075, A21247, and A-31553) for 1 h at room temperature before mounting in VECTASHIELD (Vector Laboratories; H-1200).

The in situ hybridization was processed with a standard protocol described previously (Su et al., 2011). Briefly, third instar larval wing discs with corresponding genotypes were dissected, fixed, dehydrated, hydrated, and then incubated with specific RNA probes synthesized using a Digoxigenin RNA Labeling Kit (Roche; 11175025910). Discs were incubated overnight with HRP-conjugated anti-Digoxigenin antibody (Roche; 11207733910) at 4°C followed by development using a TSA Plus Fluorescence Kit (PerkinElmer; NEL741001KT) at room temperature. Primers for RNA probe synthesis are listed in Table S2.

Images were obtained on a Leica TCS SP8 confocal microscope (Leica 20×/0.70 and 63×/1.40 oil objective lenses) or a Zeiss Axio Imager Z2 microscope (Zeiss 20×/0.80 objective lens) equipped with an ApoTome as well as an AxioCam Mrm Camera. Images were processed with LAS AF X (Leica) or AxioVision 4.8.1 (Zeiss) and Adobe Photoshop CS5 to adjust brightness and/or contrast. 3D reconstitutions were used to show the side view of fly wing discs in AxioVision 4.8.1.

Adult wings were dissected and mounted in Euparal mounting medium (BioQuip; 6372A). The images were acquired with a Leica DMIL LED inverted microscope (Leica 4×/0.10 and 10×/0.22 objective lenses) with a QImaging MicroPublisher RTV-5.0 CCD Camera (QImaging).

### Cell culture, transfection, and double-stranded RNA (dsRNA) treatment

*Drosophila* Schneider S2 cells were cultured at 25°C in Schneider's *Drosophila* medium (Thermo Fisher Scientific; 21720024) supplemented with 10% FBS (Lanzhou Bailing; 20130507) and 100 U/ml of penicillin/streptomycin (Thermo Fisher Scientific; 15140122). HEK293T cells (ATCC; CRL-1573) were maintained in DMEM (Thermo Fisher Scientific; C11995500BT) with 10% FBS and 100 U/ml of penicillin/streptomycin at 37°C with 5% $CO_2$. DNA transfections were performed using a standard calcium phosphate protocol, Effectene Transfection Reagent (Qiagen; 301425), or Lipofectamine 2000 Transfection Reagent (Thermo Fisher Scientific; 11668019). Cell cycle arrest was induced by treating HEK293T cells for 24 h with colchicine (30 µM; JiSiEnBei; JS0420).

In protein degradation assays, S2 cells were treated for up to 5 h with cycloheximide (50 mg/ml; Sigma-Aldrich; 5087390001) before harvest to inhibit nascent protein synthesis. MG132 (20 µM; Sigma-Aldrich; SML1135) was used to inhibit proteasome activity, while chloroquine (50 µM; Sigma-Aldrich; C6628) was used to inhibit lysosome function. S2 cells transfected with *hs-wdb-HA*, and indicated vectors were heat-shocked for half an hour at 37°C after transfection for 36 h. The cells were then recovered at 25°C for 1 h followed by drug treatment. 1 mM $CuSO_4$ was used to induce the expression of *PpV*, *PpV**, or *OsTIR1* cloned into *pMT* vector. 1 mM auxin (Sigma-Aldrich; I2886) was used to induce the formation of OsTIR1-SCF E3 complex.

dsRNA was generated with the RiboMAX Large Scale RNA Production System (Promega; P1280) according to the manufacturer's instructions. DNA templates targeting *PpV* (encoding amino acids 3–149), *wdb*#1 (encoding amino acids 246–346), *wdb*#2 (encoding amino acids 268–315), and *mts* (encoding amino acids 93–211) were generated by PCR and used for dsRNA synthesis. dsRNA targeting yeast *Gal80* coding sequence was used as a negative control. For RNAi knockdown in S2 cells, dsRNA transfection was performed using a standard calcium phosphate protocol. Primers used to generate dsRNAs are listed in Table S2.

### Biochemistry

S2, HEK293T cells, and third instar larval wing discs were lysed in NP-40 buffer (1% NP-40, 150 mM NaCl, and 50 mM Tris-HCl,

pH 8) or radioimmunoprecipitation assay buffer (1% Triton X-100, 0.1% SDS, 1% sodium deoxycholate, 150 mM NaCl, and 50 mM Tris-HCl, pH 7.4) supplemented with protease inhibitor cocktail (Roche; 11697498001). Phosphatase inhibitors (25 mM NaF and 400 mM $Na_3VO_4$) were added to the lysis buffer when necessary. Immunoblotting was performed using standard protocols. The following antibodies were used for immunoblotting: mouse anti-β-tubulin (1:5,000; DSHB; E7), mouse anti-human GAPDH (1:1,000; DSHB; 2G7), mouse anti-Flag (1:2,000; CMC-Tag; A0022), rabbit anti β-actin (1:1,000; ABclonal; AC026), rabbit anti-Phospho-Aurora A (Thr288; 1:500; ABclonal; AP0523), rabbit anti-GFP tag (1:1,000; Thermo Fisher Scientific; A-11122), mouse anti-HA tag (1:2,000; 6E2; CST; 2367S), mouse anti-Myc tag (1:2,000; 9B11; CST; 2276S), rabbit anti-PP2A A subunit (1:1,000; CST; 2039S), rabbit anti-PP2A C subunit (1:1,000; CST; 2038S), rabbit anti-PpV (1:2,000; generated in this study), guinea pig anti-Wdb (1:2,000; a gift of A. Sehgal), mouse anti-Ub (1:2,000; P4D1; Santa Cruz; sc-8017), mouse anti-p44/42 MAPK (Erk1/2; 1:1,000; ENZO; BML-MA1366-0025), mouse anti-Hsp60 (LK-1; 1:1,000; ENZO; ADI-SPA-806-D), and HRP-conjugated goat anti-mouse/rabbit/guinea pig IgG (H+L; 1:10,000; ABclonal; AS003, AS014, and AS025). Immunoblots presented in all figures are representatives of at least three independent experiments.

Immunoprecipitation was performed using either agarose anti-HA (Vector Labs MB-0734) or Dynabeads (Thermo Fisher Scientific; 10006D) according to the manufacturer's instructions. For ubiquitination assays, S2 cells transfected with indicated vectors were hot-lysed in denaturing buffer (1% SDS, 50 mM Tris, pH 7.5, and 0.5 mM EDTA) by boiling for 5 min. Lysates were then diluted 10-fold with NP-40 lysis buffer and subjected to immunoprecipitation. In some experiments, mutant forms of Ub ($Ub^{K48}$ or $Ub^{K63}$) were used to investigate the specificity of Ub modification on substrates. In $Ub^{K48}$ or $Ub^{K63}$, all the lysine residues were mutated to arginine residues except at amino acid position K48 or K63, which allowed the poly-Ub linkage only occurring at K48 or K63, respectively.

For phospho-protein enrichment, S2 cells were lysed in NP-40 buffer. Phospho-proteins in the lysates were then purified using PhosphoProtein Purification Kit (Qiagen; 37101) according to the manufacturer's instructions.

To measure the PP2A activity, third instar larvae were dissected, and 50–80 pairs of imaginal wing discs were collected and lysed in NP-40 buffer followed by PP2A activity measurement. Normalized PP2A activity of 1 μg wing disc protein lysate was determined by measuring phosphate release using a non-radioactive, malachite-green based Serine/Threonine Phosphatase Assay System (Promega; V2460). A synthetic phosphopeptide RRA(pT)VA was used as a specific PP2A substrate. 50 mM NaF was used to inhibit the PP2A activity.

To purify Ci ZnF protein, nucleotides encoding the zinc finger domain (amino acids 349–516) of Ci were cloned into *pGEX-6P-1* (Addgene; 27–4597-01). GST-tagged protein was purified by glutathione agarose (Thermo Fisher Scientific; 16100) in equilibration/wash buffer (50 mM Tris and 150 mM NaCl, pH 8.0). After wash, fusion protein was eluted with 100 mM glutathione in equilibration/wash buffer. Protein concentration was estimated by Coomassie-stained gels. Known concentrations of BSA were used as protein concentration standards.

For the electrophoretic mobility shift assay, purified GST-tagged Ci ZnF protein and 50 fmol biotin-labeled (or 5 pmol un-labeled "cold") double-stranded DNA probes were incubated at 25°C in 20 μl reaction buffer (20 mM Hepes, pH 7.9; 50 mM KCl; 0.1 mM EDTA; 2 mM DTT; 6 mM $MgCl_2$; 0.1 mg/ml BSA; 50 μg/ml poly[dI-dC], Thermo Fisher Scientific; 20148E; and 5% glycerol) for 30 min. The reaction mixture was loaded and resolved in 8% Tris-borate-EDTA (TBE) gel. About 400 ng of GST–Ci ZnF recombinant protein were used per reaction.

### Molecular biology

Total RNA of fly wing imaginal discs was extracted using Magzol reagent (Magen; R4801-02). Residual genomic DNA was removed by gDNA remover supplied by Promega Eastep RT Master Mix Kit (Promega; LS2050). First-strand cDNA was synthesized using oligo-dT primer (Thermo Fisher Scientific; 18418012) and SuperScript III reverse transcription (Thermo Fisher Scientific; 18080093).

HA-tagged *wdb* was generated by cloning the coding as well as the 5′ untranslated regulatory sequence amplified from *pUAST-wdb* transgenic fly (Hannus et al., 2002) into *pCaspeR-hs* vector (*Drosophila* Genomics Resource Center [DGRC]; 1215) derived from *pCaSpeR*.

The *PpV-Myc* construct was generated by fusing a Myc tag at the C terminus of the full-length *PpV* cDNA and then cloned into the *pMT* vector (DGRC; 1145).

To generate *PpV*-Myc* plasmid, two mutations (H53Q and R83A) were induced by primer-based mutagenesis (I-5; Molecular Cloning Laboratories; I5HD-200).

The full-length *PpV* and *PpV** were cloned into the *pcDNA3.1* vector (ATCC; V790-20) to generate *pcDNA3.1-PpV* and *pcDNA3.1-PpV**.

The *OsTIR1-Myc* and *mAID* were cloned from pMK289 (mAID-mClover-NeoR; Addgene; 72827) and pMK232 (CMV-OsTIR1-PURO; Addgene 72834), respectively. Then the *OsTIR1-Myc* and *mAID* were cloned into the *pMT-gfp* vector. Then the full-length *PpV* was cloned into this vector to generate *pMT-OsTIR1-Myc-P2A-PpV-mAID-gfp* vector.

The *PpV 5′-gfp* reporter construct was generated by fusing a GFP tag in frame after the *PpV* 5′ regulatory sequence (−3684 +3) and then cloned into *pB-ARE-Green* (a gift of D.P. Bohmann, University of Rochester, Rochester, NY).

To generate $Wdb^{\Delta Mts}$, nucleotides that encode amino acids 129–135, 268–270, 304–310, 351–353, and 394 were deleted from *hs-wdb-HA* plasmid.

The *AURKA-HA* construct was generated by fusing a HA tag at the C terminus of the full-length *AURKA* cDNA and then cloned into the *pcDNA3.1* vector.

The *pUAST-Myc-Ub*, *pUAST-Myc-*$Ub^{K48}$, and *pUAST-Myc-*$Ub^{K63}$ were gifts from A. Plessis (Institut Jacques Monod, Paris, France).

### Antibody generation

A rabbit polyclonal antibody was raised against a synthetic peptide (AVPDAERVIPKQNTTP) corresponding to amino acids

285–300 of fly PpV (Abclonal). Its specificity was confirmed by immunoblotting (1:1,000) and immunostaining (1:100). Note this PpV antibody was able to cross-react with human PP6C.

A rabbit polyclonal antibody was raised against full-length fly Col protein (Abclonal). Its specificity was confirmed by immunostaining (1:2,000).

### Quantification and statistical analysis

For quantification of the distance between two points in adult wing blade, the mounted wing blade was imaged, and the distance between distal ends of L3 and L4 longitudinal veins and the distance between distal ends of L2 and L5 veins were measured by QCapture Pro software (QImaging).

For quantification of the amount of PpV or Mts protein in association with Wdb after coimmunoprecipitation, the amounts of Wdb, Mts, or PpV were determined by the National Institutes of Health ImageJ software on the basis of the mean pixel intensity of each band shown in the blot. Relative amounts of PpV or Mts protein associated with Wdb were then measured by calculating the pixel intensity ratio between the PpV or Mts bands and relevant Wdb bands in each lane.

For quantification of PP2A activities, 1 µg protein lysate extracted from wing discs expressing UAS-*gfp* or UAS-*hhN* was determined by measuring phosphate release using a nonradioactive, malachite-green–based phosphatase assay system. A synthetic phosphopeptide RRA(pT)VA was used as the specific PP2A substrate. The reading from wing discs expressing UAS-*gfp* was set as 100% of the PP2A activity (basal activity).

For quantification of the intensity of antibody staining, images were taken with the same confocal settings and the mean fluorescence intensity was measured with the National Institutes of Health ImageJ software.

Two-tailed Student's *t* tests were used to analyze the difference between two different genotypes.

### Online supplemental material

Fig. S1 shows genetic interactions between *PpV* and Hh signaling components. Fig. S2 shows two degradation pathways used by exogenous Wdb protein in S2 cells. This figure also shows the alteration of Wdb protein stability upon manipulating *PpV* expression in S2 cells and in wing discs. Fig. S3 shows the phosphorylation pattern of Wdb protein in S2 cells. Fig. S4 shows the characterization of PpV antibody in immunofluorescence staining and the alteration of PpV protein abundance upon manipulating Hh signaling. Fig. S5 shows the *PpV* mRNA transcription and activity of *PpV* 5′ regulatory elements when Hh signaling was manipulated in wing discs. Table S1 shows all the genetic crosses for figures and supplemental figures. Table S2 lists all primers used in the study.

## Acknowledgments

We thank Drs. D.P. Bohmann, J. Pastor-Pareja, A. Plessis, A. Sehgal, J.E. Treisman, J.-P. Vincent, Bloomington *Drosophila* Stock Center (BDSC) at Indiana University, Bloomington, Tsinghua Fly Center at Tsinghua Universisty (THFC), Beijing, Vienna *Drosophila* RNAi Center (VDRC) at Vienna Biocenter Core Facilities, Vienna, and Developmental Studies Hybridoma Bank (DSHB) at the University of Iowa, Iowa City (created by the Eunice Kennedy Shriver National Institute of Child Health and Human Development of the National Institutes of Health and maintained at the University of Iowa, Iowa City) for fly stocks, antibodies, and plasmids. We also thank Dr. C. Shan at the National Center for Protein Science at Peking University for assistance with microscopic imaging.

This work was supported by grants from the National Natural Science Foundation of China (31725019, 31830058, and 31671512 to A.J. Zhu, and 31701274 to Y. Su), the Peking-Tsinghua Center for Life Sciences (to A.J. Zhu and M. Liu), and the Ministry of Education Key Laboratory of Cell Proliferation and Differentiation (to A.J. Zhu). J. Wang, Y. Zhang, and Y. Li, are Peking University President's Scholarship awardees. BDSC and DGRC, which are supported by the grants from National Institutes of Health P40OD018537 and 2P40OD010949, respectively, provided some fly lines used in this study.

The authors declare no competing financial interests.

Author contributions: M. Liu, A. Liu., Y. Su, and A.J. Zhu designed the study; M. Liu, A. Liu, J. Wang, Y. Zhang, Y. Li, and Y. Su performed experiments and data analyses; and M. Liu, A. Liu, and A.J. Zhu wrote the paper.

Submitted: 14 October 2020
Revised: 26 November 2020
Accepted: 2 December 2020

## References

Alon, U. 2007. Network motifs: theory and experimental approaches. *Nat. Rev. Genet.* 8:450–461. https://doi.org/10.1038/nrg2102

Apionishev, S., N.M. Katanayeva, S.A. Marks, D. Kalderon, and A. Tomlinson. 2005. Drosophila Smoothened phosphorylation sites essential for Hedgehog signal transduction. *Nat. Cell Biol.* 7:86–92. https://doi.org/10.1038/ncb1210

Atwood, S.X., M. Li, A. Lee, J.Y. Tang, and A.E. Oro. 2013. GLI activation by atypical protein kinase C ι/λ regulates the growth of basal cell carcinomas. *Nature.* 494:484–488. https://doi.org/10.1038/nature11889

Baena-Lopez, L.A., C. Alexandre, A. Mitchell, L. Pasakarnis, and J.P. Vincent. 2013. Accelerated homologous recombination and subsequent genome modification in Drosophila. *Development.* 140:4818–4825. https://doi.org/10.1242/dev.100933

Barber, K.W., and J. Rinehart. 2018. The ABCs of PTMs. *Nat. Chem. Biol.* 14: 188–192. https://doi.org/10.1038/nchembio.2572

Brandman, O., and T. Meyer. 2008. Feedback loops shape cellular signals in space and time. *Science.* 322:390–395. https://doi.org/10.1126/science.1160617

Briscoe, J., and P.P. Thérond. 2013. The mechanisms of Hedgehog signalling and its roles in development and disease. *Nat. Rev. Mol. Cell Biol.* 14: 416–429. https://doi.org/10.1038/nrm3598

Chen, Y., and G. Struhl. 1996. Dual roles for patched in sequestering and transducing Hedgehog. *Cell.* 87:553–563. https://doi.org/10.1016/S0092-8674(00)81374-4

Chen, W., J.D. Arroyo, J.C. Timmons, R. Possemato, and W.C. Hahn. 2005. Cancer-associated PP2A Aalpha subunits induce functional haploinsufficiency and tumorigenicity. *Cancer Res.* 65:8183–8192. https://doi.org/10.1158/0008-5472.CAN-05-1103

Chen, Y., S. Li, C. Tong, Y. Zhao, B. Wang, Y. Liu, J. Jia, and J. Jiang. 2010. G protein-coupled receptor kinase 2 promotes high-level Hedgehog signaling by regulating the active state of Smo through kinase-dependent and kinase-independent mechanisms in Drosophila. *Genes Dev.* 24: 2054–2067. https://doi.org/10.1101/gad.1948710

Cohen, P. 2002. The origins of protein phosphorylation. *Nat. Cell Biol.* 4: E127–E130. https://doi.org/10.1038/ncb0502-e127

Couzens, A.L., J.D. Knight, M.J. Kean, G. Teo, A. Weiss, W.H. Dunham, Z.Y. Lin, R.D. Bagshaw, F. Sicheri, T. Pawson, et al. 2013. Protein interaction

network of the mammalian Hippo pathway reveals mechanisms of kinase-phosphatase interactions. *Sci. Signal.* 6:rs15. https://doi.org/10.1126/scisignal.2004712

Crozatier, M., B. Glise, and A. Vincent. 2002. Connecting Hh, Dpp and EGF signalling in patterning of the Drosophila wing; the pivotal role of collier/knot in the AP organiser. *Development.* 129:4261–4269.

Crozatier, M., B. Glise, V. Khemici, and A. Vincent. 2003. Vein-positioning in the Drosophila wing in response to Hh; new roles of Notch signaling. *Mech. Dev.* 120:529–535. https://doi.org/10.1016/S0925-4773(03)00041-8

Denef, N., D. Neubüser, L. Perez, and S.M. Cohen. 2000. Hedgehog induces opposite changes in turnover and subcellular localization of patched and smoothened. *Cell.* 102:521–531. https://doi.org/10.1016/S0092-8674(00)00056-8

Dietzl, G., D. Chen, F. Schnorrer, K.C. Su, Y. Barinova, M. Fellner, B. Gasser, K. Kinsey, S. Oppel, S. Scheiblauer, et al. 2007. A genome-wide transgenic RNAi library for conditional gene inactivation in Drosophila. *Nature.* 448:151–156. https://doi.org/10.1038/nature05954

Domínguez, M., M. Brunner, E. Hafen, and K. Basler. 1996. Sending and receiving the hedgehog signal: control by the Drosophila Gli protein Cubitus interruptus. *Science.* 272:1621–1625. https://doi.org/10.1126/science.272.5268.1621

Ertych, N., A. Stolz, O. Valerius, G.H. Braus, and H. Bastians. 2016. CHK2-BRCA1 tumor-suppressor axis restrains oncogenic Aurora-A kinase to ensure proper mitotic microtubule assembly. *Proc. Natl. Acad. Sci. USA.* 113:1817–1822. https://doi.org/10.1073/pnas.1525129113

Guillén, I., J.L. Mullor, J. Capdevila, E. Sánchez-Herrero, G. Morata, and I. Guerrero. 1995. The function of *engrailed* and the specification of *Drosophila* wing pattern. *Development.* 121:3447–3456.

Gurdziel, K., D.S. Lorberbaum, A.M. Udager, J.Y. Song, N. Richards, D.S. Parker, L.A. Johnson, B.L. Allen, S. Barolo, and D.L. Gumucio. 2015. Identification and validation of novel Hedgehog-responsive enhancers predicted by computational analysis of Ci/Gli binding site density. *PLoS One.* 10:e0145225. https://doi.org/10.1371/journal.pone.0145225

Hannus, M., F. Feiguin, C.P. Heisenberg, and S. Eaton. 2002. Planar cell polarization requires Widerborst, a B′ regulatory subunit of protein phosphatase 2A. *Development.* 129:3493–3503.

Hosing, A.S., N.C. Valerie, J. Dziegielewski, D.L. Brautigan, and J.M. Larner. 2012. PP6 regulatory subunit R1 is bidentate anchor for targeting protein phosphatase-6 to DNA-dependent protein kinase. *J. Biol. Chem.* 287:9230–9239. https://doi.org/10.1074/jbc.M111.333708

Janssens, V., J. Jordens, I. Stevens, C. Van Hoof, E. Martens, H. De Smedt, Y. Engelborghs, E. Waelkens, and J. Goris. 2003. Identification and functional analysis of two Ca2+-binding EF-hand motifs in the B"/PR72 subunit of protein phosphatase 2A. *J. Biol. Chem.* 278:10697–10706. https://doi.org/10.1074/jbc.M211717200

Jia, J., C. Tong, B. Wang, L. Luo, and J. Jiang. 2004. Hedgehog signalling activity of Smoothened requires phosphorylation by protein kinase A and casein kinase I. *Nature.* 432:1045–1050. https://doi.org/10.1038/nature03179

Johnson, R.L., J.K. Grenier, and M.P. Scott. 1995. patched overexpression alters wing disc size and pattern: transcriptional and post-transcriptional effects on hedgehog targets. *Development.* 121:4161–4170.

Junttila, M.R., P. Puustinen, M. Niemelä, R. Ahola, H. Arnold, T. Böttzauw, R. Ala-aho, C. Nielsen, J. Ivaska, Y. Taya, et al. 2007. CIP2A inhibits PP2A in human malignancies. *Cell.* 130:51–62. https://doi.org/10.1016/j.cell.2007.04.044

Kajino, T., H. Ren, S. Iemura, T. Natsume, B. Stefansson, D.L. Brautigan, K. Matsumoto, and J. Ninomiya-Tsuji. 2006. Protein phosphatase 6 down-regulates TAK1 kinase activation in the IL-1 signaling pathway. *J. Biol. Chem.* 281:39891–39896. https://doi.org/10.1074/jbc.M608155200

Kholodenko, B.N. 2006. Cell-signalling dynamics in time and space. *Nat. Rev. Mol. Cell Biol.* 7:165–176. https://doi.org/10.1038/nrm1838

Kong, M., D. Ditsworth, T. Lindsten, and C.B. Thompson. 2009. Alpha4 is an essential regulator of PP2A phosphatase activity. *Mol. Cell.* 36:51–60. https://doi.org/10.1016/j.molcel.2009.09.025

Kong, J.H., C. Siebold, and R. Rohatgi. 2019. Biochemical mechanisms of vertebrate hedgehog signaling. *Development.* 146:dev166892. https://doi.org/10.1242/dev.166892

Lee, R.T., Z. Zhao, and P.W. Ingham. 2016. Hedgehog signalling. *Development.* 143:367–372. https://doi.org/10.1242/dev.120154

Lemmon, M.A., D.M. Freed, J. Schlessinger, and A. Kiyatkin. 2016. The Dark Side of Cell Signaling: Positive Roles for Negative Regulators. *Cell.* 164:1172–1184. https://doi.org/10.1016/j.cell.2016.02.047

Leonard, D., W. Huang, S. Izadmehr, C.M. O'Connor, D.D. Wiredja, Z. Wang, N. Zaware, Y. Chen, D.M. Schlatzer, J. Kiselar, et al. 2020. Selective PP2A enhancement through biased heterotrimer stabilization. *Cell.* 181:688–701.e16. https://doi.org/10.1016/j.cell.2020.03.038

Li, X., A. Scuderi, A. Letsou, and D.M. Virshup. 2002. B56-associated protein phosphatase 2A is required for survival and protects from apoptosis in Drosophila melanogaster. *Mol. Cell. Biol.* 22:3674–3684. https://doi.org/10.1128/MCB.22.11.3674-3684.2002

Li, S., S. Li, Y. Han, C. Tong, B. Wang, Y. Chen, and J. Jiang. 2016. Regulation of Smoothened Phosphorylation and High-Level Hedgehog Signaling Activity by a Plasma Membrane Associated Kinase. *PLoS Biol.* 14:e1002481. https://doi.org/10.1371/journal.pbio.1002481

Liu, A. 2019. Proteostasis in the Hedgehog signaling pathway. *Semin. Cell Dev. Biol.* 93:153–163. https://doi.org/10.1016/j.semcdb.2018.10.009

Liu, B., H.W. Sung, and J. Großhans. 2019. Multiple functions of the essential gene *PpV* in *Drosophila* early development. *G3 (Bethesda).* 9:3583–3593. https://doi.org/10.1534/g3.119.400662

Liu, B., I. Gregor, H.A. Müller, and J. Großhans. 2020. Fluorescence fluctuation analysis reveals PpV dependent Cdc25 protein dynamics in living embryos. *PLoS Genet.* 16:e1008735. https://doi.org/10.1371/journal.pgen.1008735

Ma, X., J.Y. Lu, Y. Dong, D. Li, J.N. Malagon, and T. Xu. 2017. PP6 Disruption Synergizes with Oncogenic Ras to Promote JNK-Dependent Tumor Growth and Invasion. *Cell Rep.* 19:2657–2664. https://doi.org/10.1016/j.celrep.2017.05.092

Maier, D., S. Cheng, D. Faubert, and D.R. Hipfner. 2014. A broadly conserved g-protein-coupled receptor kinase phosphorylation mechanism controls Drosophila smoothened activity. *PLoS Genet.* 10:e1004399. https://doi.org/10.1371/journal.pgen.1004399

Méthot, N., and K. Basler. 1999. Hedgehog controls limb development by regulating the activities of distinct transcriptional activator and repressor forms of Cubitus interruptus. *Cell.* 96:819–831. https://doi.org/10.1016/S0092-8674(00)80592-9

Mi, J., J. Dziegielewski, E. Bolesta, D.L. Brautigan, and J.M. Larner. 2009. Activation of DNA-PK by ionizing radiation is mediated by protein phosphatase 6. *PLoS One.* 4:e4395. https://doi.org/10.1371/journal.pone.0004395

Morita, K., S. He, R.P. Nowak, J. Wang, M.W. Zimmerman, C. Fu, A.D. Durbin, M.W. Martel, N. Prutsch, N.S. Gray, et al. 2020. Allosteric activators of protein phosphatase 2A display broad antitumor activity mediated by dephosphorylation of MYBL2. *Cell.* 181:702–715.e20. https://doi.org/10.1016/j.cell.2020.03.051

O'Connor, C.M., A. Perl, D. Leonard, J. Sangodkar, and G. Narla. 2018. Therapeutic targeting of PP2A. *Int. J. Biochem. Cell Biol.* 96:182–193. https://doi.org/10.1016/j.biocel.2017.10.008

Ohama, T. 2019. The multiple functions of protein phosphatase 6. *Biochim. Biophys. Acta Mol. Cell Res.* 1866:74–82. https://doi.org/10.1016/j.bbamcr.2018.07.015

Pak, E., and R.A. Segal. 2016. Hedgehog Signal Transduction: Key Players, Oncogenic Drivers, and Cancer Therapy. *Dev. Cell.* 38:333–344. https://doi.org/10.1016/j.devcel.2016.07.026

Port, F., H.M. Chen, T. Lee, and S.L. Bullock. 2014. Optimized CRISPR/Cas tools for efficient germline and somatic genome engineering in *Drosophila*. *Proc. Natl. Acad. Sci. USA.* 111:E2967–E2976. https://doi.org/10.1073/pnas.1405500111

Porter, J.A., D.P. von Kessler, S.C. Ekker, K.E. Young, J.J. Lee, K. Moses, and P.A. Beachy. 1995. The product of hedgehog autoproteolytic cleavage active in local and long-range signalling. *Nature.* 374:363–366. https://doi.org/10.1038/374363a0

Rusin, S.F., K.A. Schlosser, M.E. Adamo, and A.N. Kettenbach. 2015. Quantitative phosphoproteomics reveals new roles for the protein phosphatase PP6 in mitotic cells. *Sci. Signal.* 8:rs12. https://doi.org/10.1126/scisignal.aab3138

Sangodkar, J., C.C. Farrington, K. McClinch, M.D. Galsky, D.B. Kastrinsky, and G. Narla. 2016. All roads lead to PP2A: exploiting the therapeutic potential of this phosphatase. *FEBS J.* 283:1004–1024. https://doi.org/10.1111/febs.13573

Sanicola, M., J. Sekelsky, S. Elson, and W.M. Gelbart. 1995. Drawing a stripe in Drosophila imaginal disks: negative regulation of decapentaplegic and patched expression by engrailed. *Genetics.* 139:745–756.

Silverstein, A.M., C.A. Barrow, A.J. Davis, and M.C. Mumby. 2002. Actions of PP2A on the MAP kinase pathway and apoptosis are mediated by distinct regulatory subunits. *Proc. Natl. Acad. Sci. USA.* 99:4221–4226. https://doi.org/10.1073/pnas.072071699

Slusarski, D.C., C.K. Motzny, and R. Holmgren. 1995. Mutations that alter the timing and pattern of cubitus interruptus gene expression in Drosophila melanogaster. *Genetics.* 139:229–240.

Strack, S., J.T. Cribbs, and L. Gomez. 2004. Critical role for protein phosphatase 2A heterotrimers in mammalian cell survival. *J. Biol. Chem.* 279:47732–47739. https://doi.org/10.1074/jbc.M408015200

Strutt, H., C. Thomas, Y. Nakano, D. Stark, B. Neave, A.M. Taylor, and P.W. Ingham. 2001. Mutations in the sterol-sensing domain of Patched suggest a role for vesicular trafficking in Smoothened regulation. *Curr. Biol.* 11:608–613. https://doi.org/10.1016/S0960-9822(01)00179-8

Su, Y., J.K. Ospina, J. Zhang, A.P. Michelson, A.M. Schoen, and A.J. Zhu. 2011. Sequential phosphorylation of smoothened transduces graded hedgehog signaling. *Sci. Signal.* 4:ra43. https://doi.org/10.1126/scisignal.2001747

Tabata, T., C. Schwartz, E. Gustavson, Z. Ali, and T.B. Kornberg. 1995. Creating a *Drosophila* wing de novo, the role of *engrailed*, and the compartment border hypothesis. *Development.* 121:3359–3369.

Thompson, J.J., and C.S. Williams. 2018. Protein Phosphatase 2A in the Regulation of Wnt Signaling, Stem Cells, and Cancer. *Genes (Basel).* 9:121. https://doi.org/10.3390/genes9030121

Torroja, C., N. Gorfinkiel, and I. Guerrero. 2004. Patched controls the Hedgehog gradient by endocytosis in a dynamin-dependent manner, but this internalization does not play a major role in signal transduction. *Development.* 131:2395–2408. https://doi.org/10.1242/dev.01102

Torroja, C., N. Gorfinkiel, and I. Guerrero. 2005. Mechanisms of Hedgehog gradient formation and interpretation. *J. Neurobiol.* 64:334–356. https://doi.org/10.1002/neu.20168

Vlastaridis, P., P. Kyriakidou, A. Chaliotis, Y. Van de Peer, S.G. Oliver, and G.D. Amoutzias. 2017. Estimating the total number of phosphoproteins and phosphorylation sites in eukaryotic proteomes. *Gigascience.* 6:1–11. https://doi.org/10.1093/gigascience/giw015

Xu, Y., Y. Xing, Y. Chen, Y. Chao, Z. Lin, E. Fan, J.W. Yu, S. Strack, P.D. Jeffrey, and Y. Shi. 2006. Structure of the protein phosphatase 2A holoenzyme. *Cell.* 127:1239–1251. https://doi.org/10.1016/j.cell.2006.11.033

Xu, P., X. Lin, and X.H. Feng. 2016. Posttranslational regulation of Smads. *Cold Spring Harb. Perspect. Biol.* 8:a022087. https://doi.org/10.1101/cshperspect.a022087

Zeng, K., R.N. Bastos, F.A. Barr, and U. Gruneberg. 2010. Protein phosphatase 6 regulates mitotic spindle formation by controlling the T-loop phosphorylation state of Aurora A bound to its activator TPX2. *J. Cell Biol.* 191:1315–1332. https://doi.org/10.1083/jcb.201008106

Zhang, C., E.H. Williams, Y. Guo, L. Lum, and P.A. Beachy. 2004. Extensive phosphorylation of Smoothened in Hedgehog pathway activation. *Proc. Natl. Acad. Sci. USA.* 101:17900–17907. https://doi.org/10.1073/pnas.0408093101

Zhu, A.J., L. Zheng, K. Suyama, and M.P. Scott. 2003. Altered localization of Drosophila Smoothened protein activates Hedgehog signal transduction. *Genes Dev.* 17:1240–1252. https://doi.org/10.1101/gad.1080803

# Supplemental material

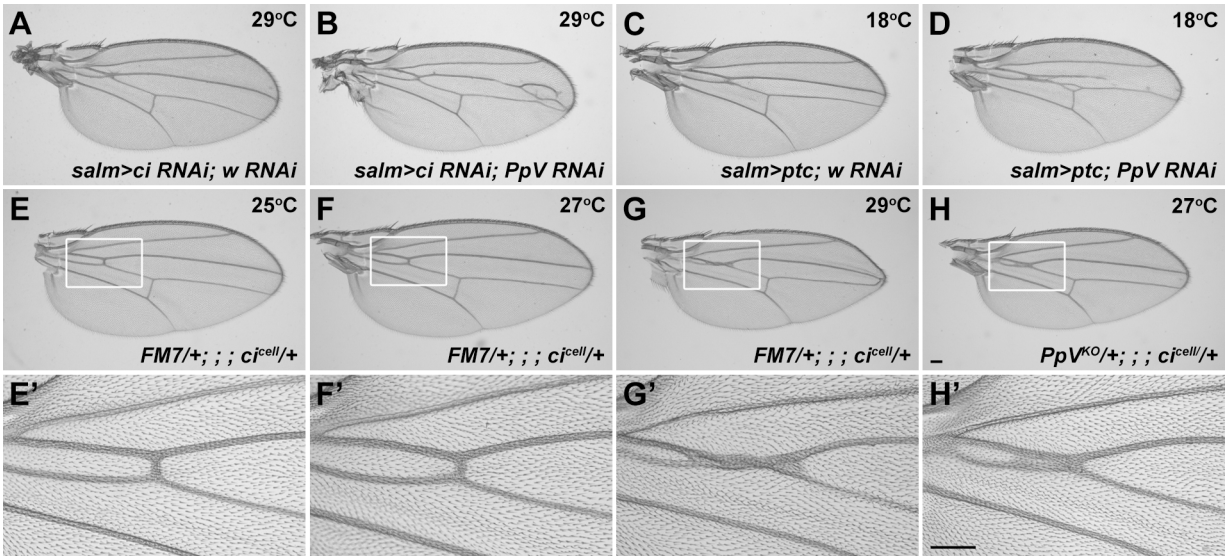


Figure S1. ***PpV* genetically interacts with Hh signaling. (A–D)** Overexpressing *ci RNAi* (A) or *ptc* (C) by *salm*-Gal4, which expressed primarily between L2 and L5 longitudinal veins in the wing blade, resulted in shortened anterior cross vein (ACV) and reduced distance between L3 and L4 veins. Knocking down *PpV* by RNAi further enhanced the defects caused by *ci* RNAi or *ptc* overexpression alone (B and D). **(E–H′)** Heterozygous $ci^{cell}$ mutant adult wings displayed typical loss of Hh signaling phenotypes: fusion of L3 and L4 veins at proximal ends, shortened ACV, and reduced distance between L3 and L4 veins. These phenotypes became increasingly apparent as culture temperature rose from 25°C to 29°C (E–G). Note the size of corresponding wing blade became progressively smaller. At 27°C, heterozygous $PpV^{KO}$ (H) dominantly enhanced heterozygous $ci^{cell}$ phenotype (F) to the same degree as that shown by $ci^{cell}$ alone at 29°C (G). E′, F′, G′, and H′ are enlarged images of boxed regions in E, F, G, and H. Scale bars, 100 µm.

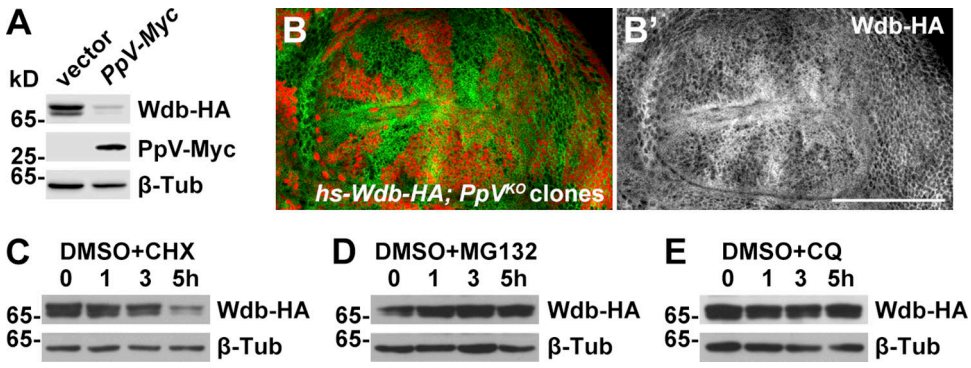


Figure S2. **PpV regulates exogenous Wdb protein stability. (A)** Exogenous Wdb-HA protein production controlled by an *hs* promoter (*hs*-Wdb-HA) was reduced when *PpV* was overexpressed in S2 cells as shown by immunoblotting. β-Tubulin served as the loading control for all experiments. **(B and B′)** *hs*-Wdb-HA was strongly elevated in loss-of-function $PpV^{KO}$ somatic clones (marked by the absence of RFP). Note uniform expression pattern of *hs*-Wdb-HA shown in Fig. 3 E. **(C–E)** Nascent Wdb protein displayed a half-life around 3 h in S2 cells (C). Treatment of S2 cells with either proteasome inhibitor MG132 (D) or lysosome inhibitor chloroquine (CQ; E) was able to prevent the degradation of Wdb protein. Scale bar, 100 µm.

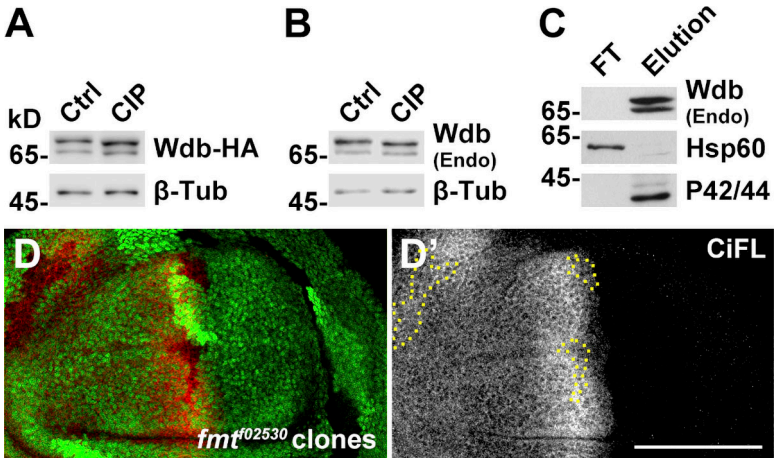


Figure S3. **Wdb protein is phosphorylated in vivo. (A and B)** Both endogenous (B) and exogenous Wdb protein (A) migrated as a doublet as shown by immunoblotting. Upon the treatment with calf intestine phosphatase (CIP), both bands of exogenous (A) or endogenous (Endo; B) Wdb protein in S2 cell lysates migrated faster than those in untreated lysate. **(C)** After purification using a PhosphoProtein purification kit (Qiagen), phosphorylated proteins in the S2 cell lysates were enriched and then collected in the elution. As shown by immunoblotting, the Wdb antibody recognized both bands of the Wdb protein, indicating that the endogenous Wdb protein was hyper-phosphorylated. Hsp60 and the MAPK P42/44 were used as controls to monitor the purification efficiency. Hsp60, which was not phosphorylated, only existed in the flow-through (FT), while P42/44 subjected to intensive phosphorylation was copurified as Wdb protein in the elution. **(D and D')** There was no obvious change on CiFL stabilization in loss-of-function *fmt*$^{f02530}$ somatic clones induced in the wing disc, which were negatively marked by the expression of GFP. Dotted lines mark the *fmt*$^{f02530}$ somatic clones. Scale bar, 100 µm. Ctrl, control.

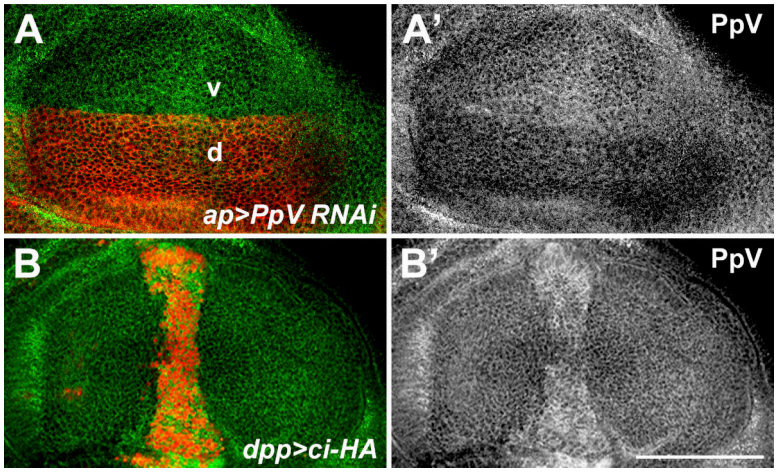


Figure S4. **PpV is regulated by the Hh signaling. (A and A')** *PpV RNAi* driven by *ap*-Gal4 in dorsal (d) compartment of the wing disc specifically reduced the protein production of PpV. The endogenous PpV was recognized by a polyclonal rabbit antibody generated in this study. **(B and B')** Overexpression of *ci* along the a-p boundary of the wing disc by *dpp*-Gal4 strongly elevated the protein production of PpV. Scale bar, 100 µm. d, dorsal; v, ventral.

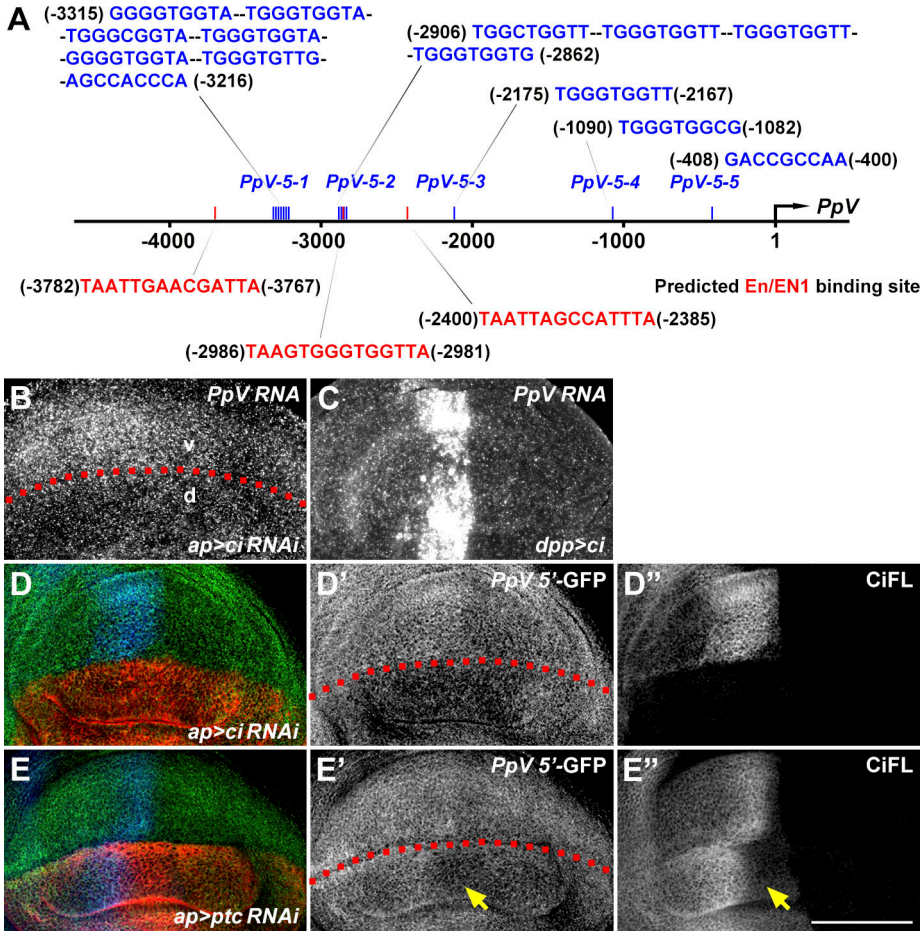


Figure S5. ***PpV* transcription is regulated by the Hh signaling. (A)** The DNA sequence of each putative Ci/Gli consensus binding site as well as predicted En/EN1 binding sites at the 5′ genomic region of the *PpV* gene locus are shown. **(B)** *ci RNAi* driven by *ap*-Gal4 in dorsal compartment of the wing disc reduced *PpV* transcription as revealed by in situ hybridization. The d-v boundary is marked by a dotted red line. **(C)** Overexpression of *ci* abutting the a-p boundary of the wing disc by *dpp*-Gal4 strongly elevated *PpV* transcription as revealed by in situ hybridization. **(D–D′′)** *PpV RNAi* driven by *ap*-Gal4 in dorsal compartment of the wing disc resulted in reduced expression of *PpV 5′*-GFP reporter. **(E–E′′)** The activity of the *PpV 5′*-GFP reporter was not activated by high-level Hh signaling in the expanded region (yellow arrows) labeled by labile CiFL when *ptc* activity was reduced by RNAi in dorsal compartment of the wing disc. Scale bar, 100 µm. d, dorsal; v, ventral.

**Provided online are two tables. Table S1 shows genetic crosses for figures and supplemental figures. Table S2 lists primers used in this study.**